DEPOSITION OF ORGANIC THIN FILMS USING ENERGY TUNABLE MOLECULAR BEAMS ON SILICON DIOXIDE AND OCTADECYLTRICHLOROSILANE MODIFIED SILICON DIOXIDE

A Thesis

Presented to the Faculty of the Graduate School

of Cornell University

In Partial Fulfillment of the Requirements for the Degree of

Master of Science

by

Jared Lynn Mack

August 2006

ABSTRACT

Organic semiconductors, in particular organic thin-film transistors (OTFTs), have been gaining recognition and spurring development in the electronics world now for more than a decade. The use of organic semiconductors is playing an ever increasing role in today's industrial research in an effort to fill niches in technology left behind by traditional semiconductors such as silicon.

The vast majority of research leading this outreach has been limited to the capabilities of thermally evaporated deposition techniques. A more advanced approach to investigating the underlying growth mechanics of organic semiconductors employs the use of a tunable molecular beam. Through controlling the expansive parameters of a molecular gas, a supersonic beam for molecular deposition can be created with strict control over the incident kinetic energy.

This supersonic beam technique was employed to study the growth characteristics of pentacene and how they pertain to the electrical properties of an organic semiconducting device. At a constant growth rate, films were deposited at three incident kinetic energies (1.5 eV, 2.7 eV, 4.5 eV, and 6.7 eV) and analyzed using ellipsometry and atomic force microscopy. Growth characteristics of the film (roughening exponent α, growth exponent β, and the correlation length) were then extracted. Finally, surface modification of the dielectric with the self-assembled monolayer (SAM) octadecyltrichlorosilane (OTS) was used to influence the nucleation and growth parameters of the pentacene film. These parameters were studied as a function of the incident kinetic energy and electrical properties that resulted.

BIOGRAPHICAL SKETCH

Jared Lynn Mack was born in Rugby, North Dakota on March 30, 1980. He attended Rugby High School where he excelled in math and the science as well as proved to be a strong competitor in the state wrestling competition placing 6^{th} and 5^{th}. Throughout his undergraduate career, he was involved in many research activities most significant of which was a research experience for undergrads, REU, at Cornell University under Prof. George G. Malliaras. In 2003, he graduated Augsburg College with Bachelors degrees in physics and chemistry with a minor in mathematics.

Directly following his undergraduate studies, Jared switched gears and entered into the Department of Materials Science and Engineering at Cornell University. Here, he joined the Engstrom Research Group, ERG, under the guidance of Prof. James R. Engstrom where he spent three years exploring surface science pertaining to organic semiconductor technology.

Upon receiving his Masters of Science degree, Jared again plans to switch gears and enter the Peace Corps where he will be stationed in Tanzania working on agricultural development.

ACKNOWLEDGEMENTS

Foremost, I would like to thank Prof. James R. Engstrom, who has provided me the invaluable opportunity to pursue my degree under his guidance. I feel privileged to have been a part of his meticulous pursuit of fundamental science in which his exhaustive scientific analysis distinguishes him above other professors. On a personal note, I would like to thank him for his patients and support as I struggle through a major transition in my life. I am very thankful to my minor committee member, Prof. George G. Malliaras, who has mentored me through my undergraduate research project, recommended my admittance to Cornell and has aided me as a motivating advisor since.

I owe many thanks to my lab mate Dr. Aravind Killampalli for teaching me the ropes of vacuum technology upon my entrance into the ERG group. A special thanks to Abhishek Dube and Manish Sharma who have ridden with me on all of my ups and downs in the group and especially Abhishek who has served as my technical advisor and hand holder through day to day issues.

Personally, I would like to thank my family and in particular my parents who have instilled in me the importance of working towards something you value and having the drive to accomplish it. Graduate school would be intolerable if it wasn't for the support of friends. Poorna Praveen Rajendran, Baski Gandapoueworursubmarine and Dr. Badri Velamur Asokan have supported me through what I like to call a lockbox. And finally a special thanks to Stephanie Lee who has taught me the importance of Canada and all the lessons in strategery.

TABLE OF CONTENTS

LIST OF FIGURES

LIST OF TABLES

1 Introduction

1.1 Progression of the industry

You could say an industry was born, when in 1947 John Bardeen and Walter Brattain working at Bell Labs attached gold leads to the famously depicted triangular cut piece of germanium thus creating the first semiconductor device. Following this spark, the next two decades, with inventions such as the p-n junction, the solar cell, the metal oxide semiconductor field effect transistor (MOSFET), and the laser, helped lay the groundwork for what has become known today as the technological revolution. Due to this field's immense potential in virtually every realm of human existence, industrial and governmental organizations invested its top resources, soon to be known as the fathers of the field, to hurdle the obstacles that were soon to approach them. For instance, packaging became a major limiting factor. The Bardeen's and Brattain's rudimentary transistor needed much refinement before it would become a practical commodity. The race was on in industry to find the most creative and innovative solutions to these problems. Helping set the pace for this development was Gordon Moore[1], co-founder of Intel, who coined the term "Moore's Law" which states that industry is predicted to double the number of transistors per square inch of integrated circuit every year. Lofty goals they were, but the field has met these expectations and maintained a doubling rate every eighteen months for the past 50 years. Along with creating smaller and faster circuitry, the industry has had much success diversifying to accommodate most aspects of societal interests ranging from low-cost disposable electronics to biologically integratable systems.

1.2 Organic semiconductors

Organic semiconductors, in particular organic thin-film transistors (OTFTs), have been gaining recognition and spurring development in the electronics world now for more than a decade. While the electronic performance of organic semiconductors such as charge mobility will never rival those of single-crystalline semiconductors, they possess other characteristics that are filling various niches in industry where maximum output is not the main focus. Two of the major features drawing attention to OTFTs is their significantly lower fabrication temperature and reduced production costs. Both of these help broaden the scope of application in ways that include technologies such as smart cards, electronic paper, and flat panel displays.

Often times, the electronic properties of semiconductors greatly depend on obtaining a high quality crystalline structure. Traditionally, silicon has been used as the hegemonic semiconductor owing much of its usefulness to our ability to create high-purity highly-crystalline thin films. However, the processes that are currently used create other issues; foremost is the high temperature required for crystallization, typically about 1100 °C. This is a major limiting factor in producing large area and mechanically flexible electronics in which the semiconductor would ideally be deposited on unconventional substrates. Many organics on the other hand crystallize at much lower temperatures, even as low as room temperature, allowing for a much larger variety of substrate possibilities. Of major interest is the deposition of OTFTs on polymeric surfaces. This is driven by the potential to produce light-weight, flexible and inexpensive electronics. Other novel devices such as active matrix liquid crystal displays (AMLCDs) and active matrix organic light emitting diode displays can be created by incorporating these devices with

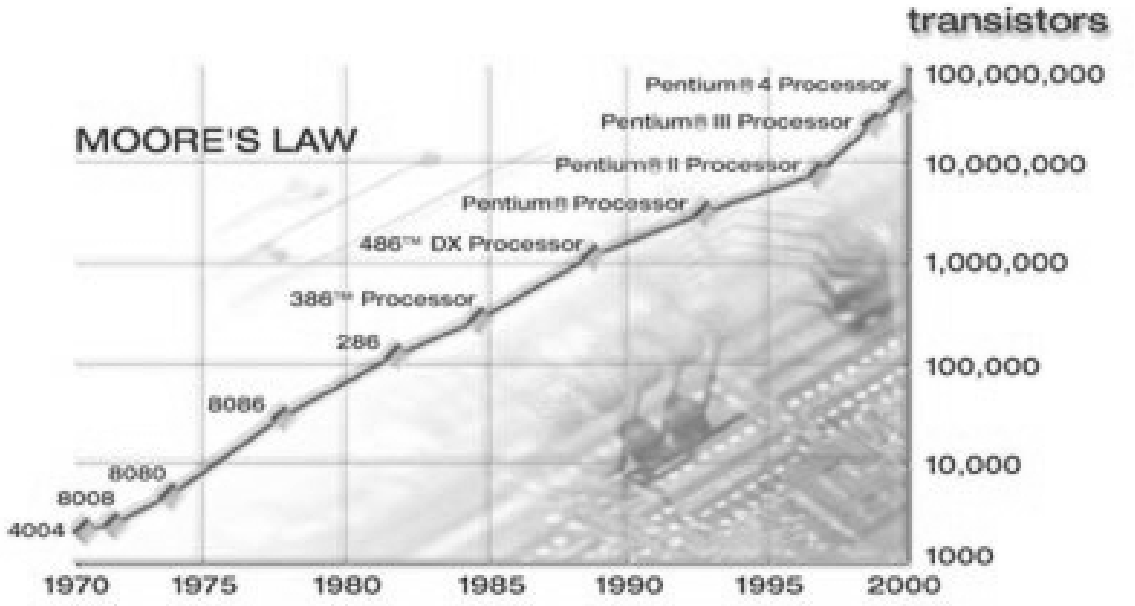

Figure 1-1 Gordon Moore in 1965 predicted that the number of transistors per given area would double every year. Borrowed from Intel Corporation's website.

either liquid crystal materials or organic light emitting diodes (OLEDs). Also, there is currently a large push to develop one-step synthesis processes using solution-based fabrication. Technologies such as spin-coating and inkjet deposition[2] are taking advantage of certain organic's solubility capabilities[3] for low cost production of organic integrated circuits.

1.2.1 Pentacene thin-film transistors

To date, most of the successful industrial development of organic semiconductors has been directed towards using either conjugated polymers or small organic molecules in creating electroluminescent diodes[4,5] and OTFTs[6,7]. Small organic molecules are oftentimes favored due to their higher charge-carrier mobilities, their ability to form ordered thin-films, and their high vapor pressures which are needed for vapor deposition. Pentacene in particular has stood out because it has demonstrated an exceptionally high transport mobility[8] which has been reported greater than 1.5 cm^2-V^{-1}-s^{-1}. This has warranted significant industrial attention, because it surpasses the mobility of the conventional inorganic semiconductor, amorphous silicon with its mobility about 1 cm^2-V^{-1}-s^{-1}. Much of the success achieved with pentacene is due to its chemical and thermal stability and also because it's planar shape helps facilitate crystalline packing.

Pictured in Figure 1-2, pentacene is a chain-like molecule consisting of five aromatic benzene rings linked linearly. This short flat geometry allows for easy crystallization into a herringbone configuration[9] forming a triclinic crystalline structure. X-ray diffraction experiments have reported that pentacene exists in two forms termed the bulk phase in which there are two polymorphs[10,11] and the thin-film phase[12]. Both of which possess the triclinic arrangement differing

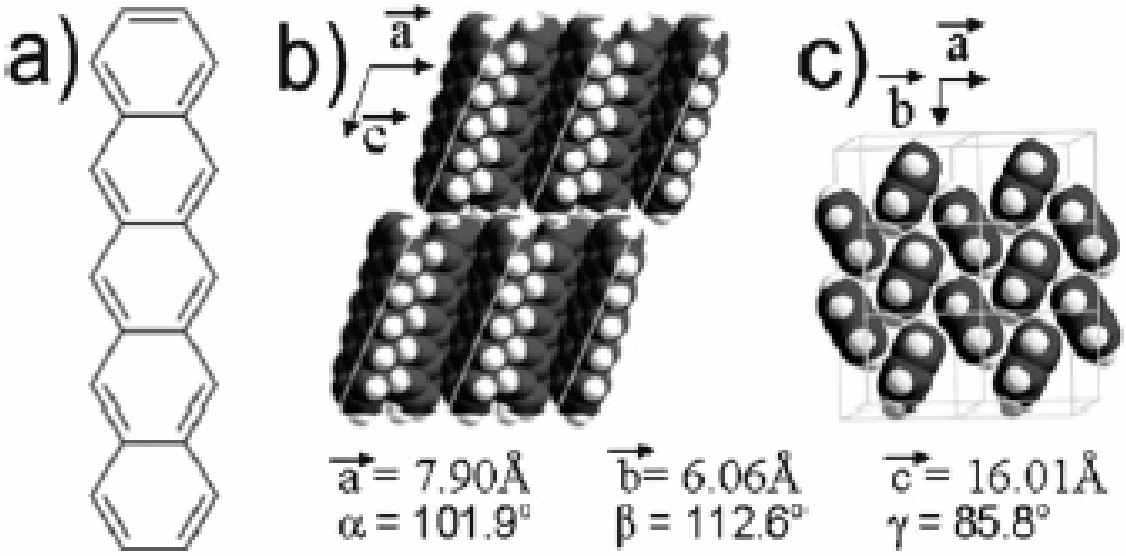

Figure 1-2 The pentacene molecule consists of benzene rings fused in a rod like structure.

only in inter-planar spacing. Industrial demand has recently focused considerable attention on the morphology and more importantly the controlled formation of this thin-film phase. This is of great importance because it is the way in which the molecule's aromatic rings arrange that determines the quality of the films charge transfer. Benzene rings in general act to delocalize the electrons of a molecule away from the core atoms. This has an amplified effect in pentacene where the herringbone crystal structure leads to aligned regions of delocalized charge thus facilitating charge mobility through the film.

1.2.2 Surface modification

The deposition conditions at the onset of film growth and the interaction between substrate and the depositing molecule are critical to the performance of electrical devices. It is in these first few monolayers of growth where the crystalline properties, which are dependent on the substrate-semiconductor interface, will give the greatest contribution to the device's charge transport. Changing the chemical properties of the surface prior to semiconductor deposition will have a profound effect on the chemical and physical bonds formed at that interface and therefore largely influence the crystalline arrangement.

The MOSFET, which is illustrated Figure 1-3, is having particular success in employing pentacene as its organic semiconductor. For these transistors to achieve high mobilities, a crystalline semiconductor film would need to be grown with low defect and grain boundary densities as well as high purity. Ideally, the entire thin film of semiconductor would entail a single crystal of pentacene eliminating any grain boundary charge trapping effects. However, due to current industrial standards of using silica (SiO_2) as the

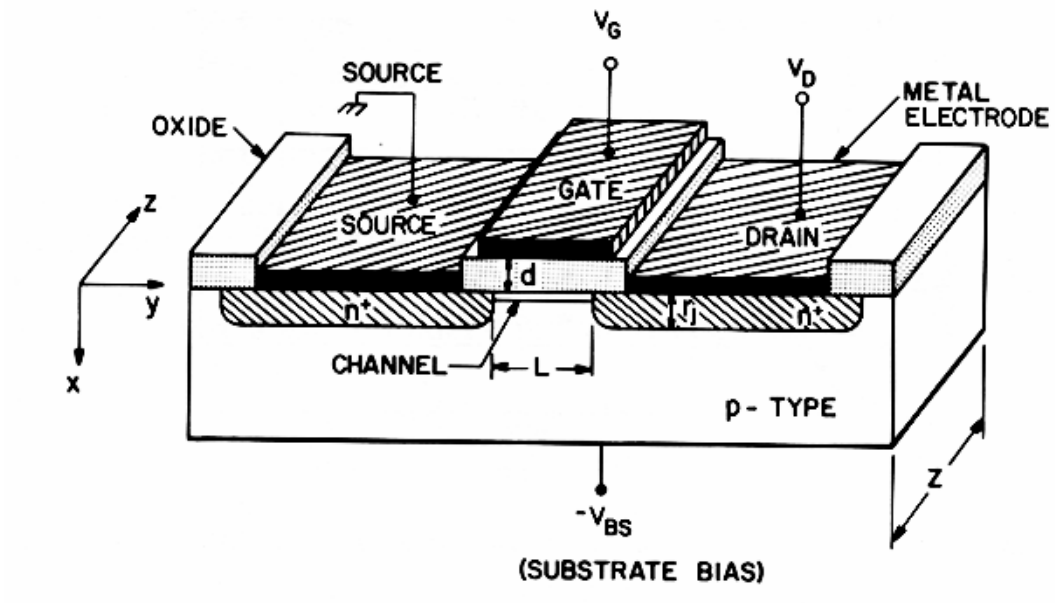

Figure 1-3 The structure of a metal oxide semiconductor field effect transistor.

dielectric of choice, polycrystalline organic films are typically made use of with varying degrees of optimization. Because most of the charge transfer in these transistors occurs near the semiconductor-dielectric interface, understanding the factors controlling the nucleation and growth of these first few layers, such as substrate surface energy and topology, is extremely important to the device's electronic properties. Recently many studies have involved modifying silica's surface characteristics through the deposition of a self-assembled monolayer (SAM) and observing the change in film morphology and charge transfer. The use of SAMs guaranties that the chemical properties of the surface are modified without changing the roughness of the surface.

A SAM, pictured in Figure 1-4, generally consists of three components; an active headgroup which binds to a suitable substrate, a tailgroup which can be terminated with a wide variety of surface functional groups and the backbone which permits the ordering of a layer by van der Waals interactions with neighboring molecules. SAMs, which can be grown by means of chemical or vapor deposition, commonly have a headgroup consisting of a silane-based organic molecule such as Hexamethyldisilozane (HMDS) and n-octadecyltrichlorosilane (OTS, Cl_3-Si-(CH_2)-CH_3). Brzoska et al.[13] describes a possible mechanism by which OTS, a long hydrocarbon chain with a trichlorosilane (-$SiCl_3$) head group, is grafted onto the polar –O-H terminated surface of the silica dielectric. Summarized in Figure 1.4, a densely packed uniform monolayer of vertical chains is deposited in a four step process; adsorption of OTS onto a thin layer of water residing on the dielectric surface, hydrolysis of the trichlorosilane head groups forming trisilanols, reorganization of silanes enabled by the physisorption on a fluid surface, and finally the formation of a 2D polysiloxane network chemically bonded to the substrate.

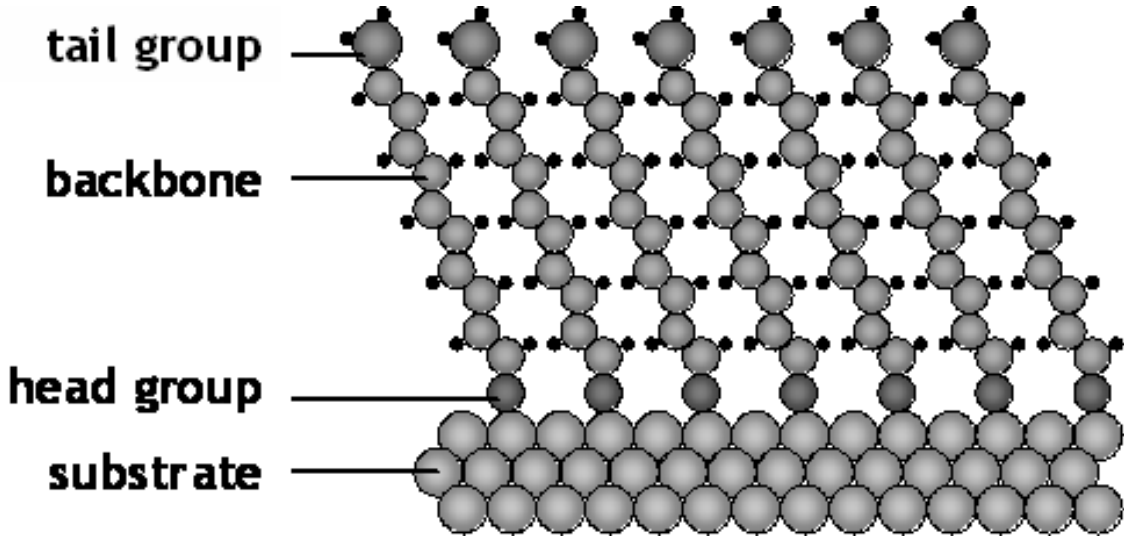

Figure 1-4 A SAM consists of a headgroup which binds to the substrate, a tailgoup which is tailored to the application and a backbone which allows for ordering throughout the layer.

Large mobility improvements, as much as a factor of 2 to 5, have been seen using this OTS surface modification[14,15].

One explanation for this phenomenon is that because the OTS-modified surface is more hydrophobic, there is a decrease in the pentacene-substrate interaction creating a more relaxed crystalline film with higher molecular ordering. These results defend theories on the importance of the first few monolayers and spurs expectations of greater electrical improvements with more investigation into the effects of SAMs. A more complete knowledge base of the organic crystal's morphological formation and charge transferring processes could lead to an enhanced and more reproducible field-effect mobility and on/off ratio, the tailoring of surface properties with appropriate SAMs for specific application, and a smoother transition of the deposition of organics onto unconventional substrates e.g. glass, polymer, fabric.

1.3 Molecular beams

With vapor deposition being a major industrial deposition technique, there is a strong drive to understand the relationship between the molecule's circumstantial internal energy state and the effect those states have in the growth of the film and its characteristic properties. Moreover, using this knowledge to tailor specific electrical properties into the thin film. For the past 30 years, molecular beams have proven very effective examining the gas-surface interactions. These molecular beam techniques are especially valuable in the case of an organic vapor deposition where the molecule's often time complicated symmetries and irregular electrical properties lead to complex interactions.

1.3.1 Characterization of molecular beams

A molecular beam refers to a collimated flow of molecules usually created through the injection of a vapor from an environment of high pressure to one of a significantly lower pressure. Most of the characteristics of the beam are determined by the high pressure region and the way in which the stream passes to that of low pressure. By and large, molecular beams are categorized as either effusive or supersonic in nature depending on the operating conditions and nozzle geometries. One standard of differentiating them is in their Knudsen number (Kn), a ratio of the beams mean free path (λ) to the characteristic length of the system (d), in this case the diameter of the orifice:

$$Kn = \frac{\lambda}{d}$$

For comparison, an effusive beam exists when Kn >> 1 signifying molecular flow while a supersonic beam entails continuum flow and has a Kn << 1.

1.3.2 Effusive molecular beams

Effusive molecular beams are commonly used in surface science analysis and for thin film deposition techniques due to the ease at which they can be produced and characterized. This follows from both the weighted velocity distribution, *I(v)*

$$I(v) = \left(\frac{2}{\alpha^4}\right) v^3 \exp\left(-\frac{v^2}{\alpha^2}\right)$$

and the flux distribution, F_i

$$F_i = \frac{P_n}{\sqrt{2\pi m k_B T_n}} \frac{\pi r_n^2}{\pi x^2} \cos\theta$$

being modeled by Maxwell Boltzmann statistics. Here, $\alpha^2=2K_BT_n/m$, P_n is the source pressure, r_n and T_n are the nozzle radius and temperature, and x is the distance between the source and the substrate.

Pointing out one of the major fallbacks to using effusive beams, the average translational energy $<E_i>$ of the beam can be calculated to be $2K_BT_n$ which at temperatures as high as several hundred ˚C is only a few meV. Other disadvantages include; a wide beam energy distribution, difficulties achieving a high flux, and poor beam to background ratio.

1.3.3 Supersonic molecular beams

Supersonic molecular beams while more complicated are more effective in probing gas-surface interactions and chemical kinetics due to a narrower velocity distribution, a peaked flux distribution, tunable translational kinetic energies, and significantly higher flux capabilities. The creation of a supersonic beam, illustrated in Figure 1-5, differs from that of an effusive beam in that there are many intermolecular interactions throughout the beam expansion. The expansion itself, an adiabatic (isentropic) process, governs the transfer of random thermal energy (rotational and vibrational) to that of translational kinetic energy directed down the beam line. The Bernoulli's equation shown below explains this. It uses the conservation of energy to relate the enthalpy

a) Effusive beam

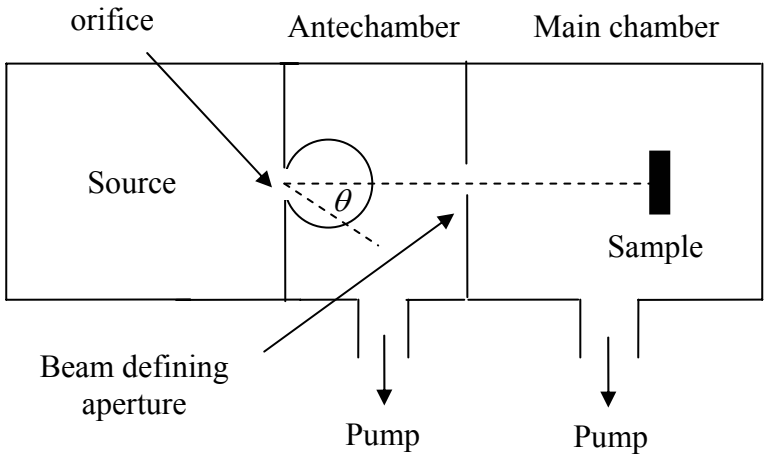

b) Supersonic beam

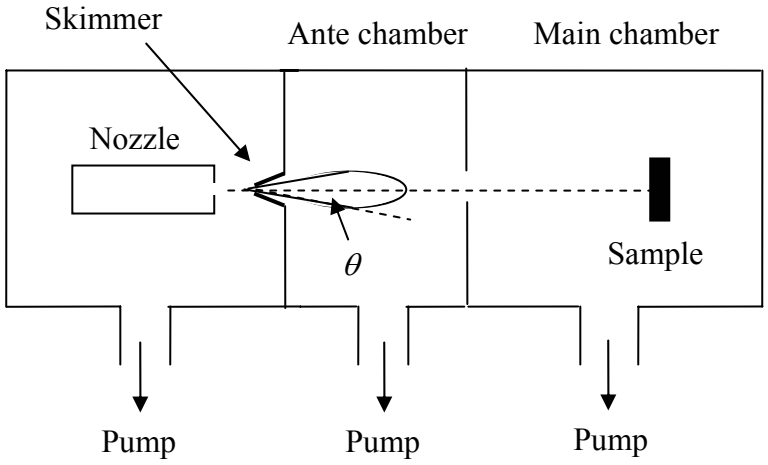

Figure 1-5 Schematic representation of molecular beams: a) effusive and b) supersonic. The closed curves downstream of the orifice and the skimmer represent the relative intensity distribution.

under stagnation conditions within the nozzle, h_0, to the enthalpy per unit mass, h, along any streamline from the nozzle plus the energy associated with the translation of the molecules, $V^2/2$.

$$h + \frac{V^2}{2} = h_0$$

As the gas expands through the orifice, it experiences a decrease in enthalpy which can be accounted for by the beams drop in pressure and temperature. The molecules encounter fewer and fewer intermolecular collisions creating a stream with a narrow flux weighted velocity distribution:

$$I(v) = N(c,\alpha)v^3 \exp\left(-\frac{(v-c)^2}{\alpha^2}\right)$$

Here, N(c,α) is a normalization constant, and c is the most probable velocity, defined as:

$$c = \left[\frac{2\gamma k_B T_n}{(\gamma - 1)m}\right]^{0.5}$$

As before, T_n is the nozzle temperature while $\gamma = C_p/C_v$, and α^2 is the standard deviation of the velocities. The resultant beam has a centerline flux that is 2-3

times higher than the effusive beam and the angular distribution is peaked with a $\cos^4\theta$ distribution for a pure gas under ideal conditions.

In creating a supersonic beam rather than an effusive one, some conditions need to be met. For instance, the following equation determines the minimum requirement for the ratio between the pressure upstream from the nozzle, P_0, to that of the downstream, P_1,

$$\frac{P_0}{P_1} \geq \left[\frac{(\gamma+1)}{2}\right]^{\frac{\gamma}{(\gamma-1)}}$$

This condition determines whether the beam will reach the speed of sound, $s = (\gamma b_B T_n/m)^{0.5}$. Above this, the beam expands supersonically, however, if it falls short an effusive beam will emerge following a Maxwell-Boltzmann distribution.

Further enhancement of the flow can be attained by seeding the vapor of interest in an inert carrier gas. In doing this, the kinetic energy of the beam can be both increased by orders of magnitude and tuned to a specific energy. Generally, the reactant gas is seeded in a dilute bath of a much lighter carrier gas such as H_2 or He. The supersonic expansion has the effect of accelerating the molecules to the mean velocity rather than the mean energy. Assuming ideal gasses with ideal molar heat capacities, the kinetic energy can be modeled as:

$$< E_i >= \frac{m_i}{< m >} < C_p > T_n$$

This is significant in that the ratio of mass of the reactant gas, m_i, to the mole fraction mean mass, <m>, is the factor by which the energy of the reactant is increased. For the case where the reactant is seeded dilutely, this ratio can be approximated by ratio of the two components molecular weights. This is a calculation bases on ideal conditions, however, it would be correctly used as an upper limit on the translational energy.

Illustrated in Figure 1-6, the supersonic expansion of a gas into vacuum is accompanied by a complex assortment of pressure gradients that need to be avoided. At the end of the expansion, molecules are traveling in excess of the speed of sound, the speed at which information travels. This situation does not allow for the molecules to adjust to the boundary conditions downstream of the expansion and shockwaves begin to form. In application, a skimmer is used to extract the expanded portion of the gas in the "zone of silence" before the onset of shockwaves.

The skimmer itself is conical or trumpet shaped with a small (150 μm) aperture to be place in close proximity to the nozzle (~ 5mm). The aperture itself is precision milled in order to minimize disturbances with the expanded gas. Its shape helps to divert away the excess free jet stream into the rest of the chamber where it can be pumped away. This greatly reduces background scattering. The extracted centerline is a well collimated that is spatially well defined and has a narrow energy distribution.

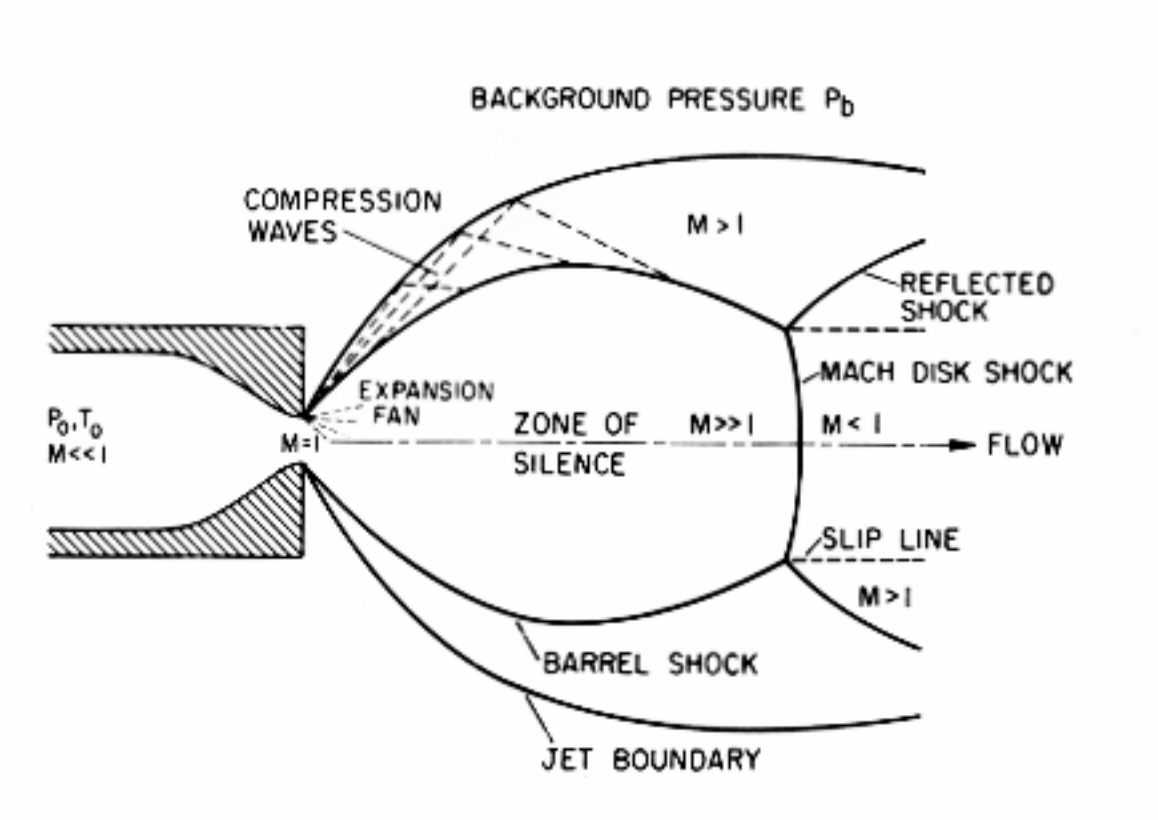

Figure 1-6 The figure shows what is commonly known as a "Free Jet" expansion which is produced without any downstream structures affecting the boundary conditions of the expansion.

1.4 Surface analysis

Much insight into the physical characteristics of thin-film semiconductors that industrial demand cares about can be gained from a look at the morphological surface changes that occur through the film's growth. Atomic Force Microscopy (AFM) has proven to be a useful tool in performing nanoscale topological assessments of films. This combined with beam deposition techniques can allow for a unique "snap-shot" look at film growth at incremental units of time.

In describing this morphological evolution, two fundamental factors are predominately used; first of which is the interface width, *w*. The interfacial width is measure of the average depth or rather the roughness of a surface. When computed by the equation

$$w = \left| \frac{1}{N} \sum_{i=1}^{N} (h_i - h_{mean})^2 \right|^{1/2},$$

the interfacial width is the standard deviation or root-mean-square (RMS) of the surface height. Here, N is the number of data entry points, h_i is the height of the N_i^{th} point, h_{mean} is the average height of all points above an arbitrary origin. This form of the interfacial width works conveniently for AFM analysis which does not use absolute values.

The second basic parameter of interest is the lateral correlation length, ξ, which is a measure of the spatial periodicity of the film. The correlation length helps refine the description of the surface by relating the grain size and distribution across the film. The lateral correlation length is given by the equation:

$$\xi = \exp\left\{\frac{\ln\left[PSD(1/L)\right] - \ln K_0}{\gamma}\right\}$$

Here the PSD is the power spectral density which is easily attained from an AFM image. A typical one-dimensional PSD (1DPSD) for pentacene, Figure 1-7, can be divided up into two distinct regions; an uncorrelated low spatial frequency region, and a frequency dependent self-affine region. It is the inverse of the special frequency dividing these two regions that defines the correlation length.

According to dynamic scaling theory, two exponential parameters (α, β) can be used to scale the interfacial width and correlation length with deposition time. Both α and β are predicted to scale time to w and ξ according to:

$$w(t) \sim t^{\beta}$$

$$\xi(t) \sim t^{\beta/\alpha}$$

With these relations, α and β, also known as the roughening and growth exponents, can be used to help predict the growth mechanism of the film.

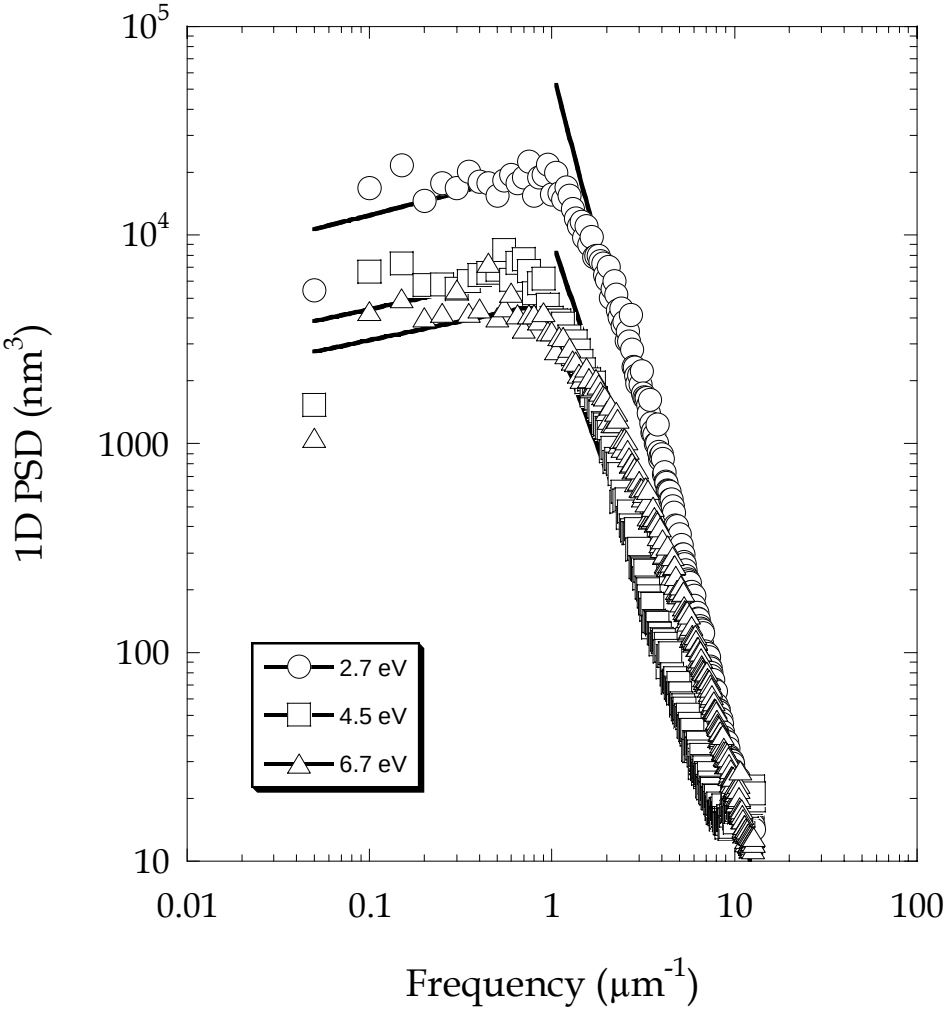

Figure 1-7 Evolution of the one dimensional power spectral density (1DPSD) as a function of spatial frequency for the three incident kinetic energies (2.7 eV, 4.5 eV, 6.7 eV) at normal incidence. Best fit lines yielding parameters K_0 and γ are shown within the self–affine data range.

2 Experimental setup

2.1 Chamber design

The deposition occurs in an ultra-high vacuum (UHV) system which consists of four individually pumped chambers; source, ante, deposition, and loadlock as illustrated in Figure 2-1 and Figure 2-2. The deposition chamber which houses the substrate during film growth is pumped using a 400 L-s^{-1} magnetically levitated turbomolecular pump (Osaka TG 403M) which maintains a base pressure of 5x10^{-10} Torr and 6x10^{-7} Torr during beam exposure. For use in beam analysis, the deposition chamber employs a Hiden 3F/EPIC (300 amu) quadrupole mass spectrometer (QMS) mounted line-of-site to the incoming beam. The QMS is aided during beam exposure by a liquid nitrogen (LN2) cooled cryo pump mounted coaxial to the beam. Substrates are mounted on a custom designed sample manipulator allowing 5 degrees of freedom (x, y, z, translational movement and polar and azimuthal rotation) as well as heating and cooling capabilities. As shown in Figure 2-1, the sample manipulator translates vertically between the load-lock and deposition chambers. Also, a chromel-alumel (K-type) thermocouple is attached to the back of the manipulator in order to monitor substrate temperatures. The load-lock, which is used to isolate the rest of the system from the external environment during sample loading, is pumped using a 300 L-s^{-1} magnetically levitated turbo pump (Seiko STPH 300C) and reaches a base pressure of 5x10^{-9} Torr in about 12 hours. Here the substrate holder is attached to the sample manipulator using a transfer arm and fork of the STLC (Thermionics) type transfer system. The manipulator is designed to accommodate samples up to 4

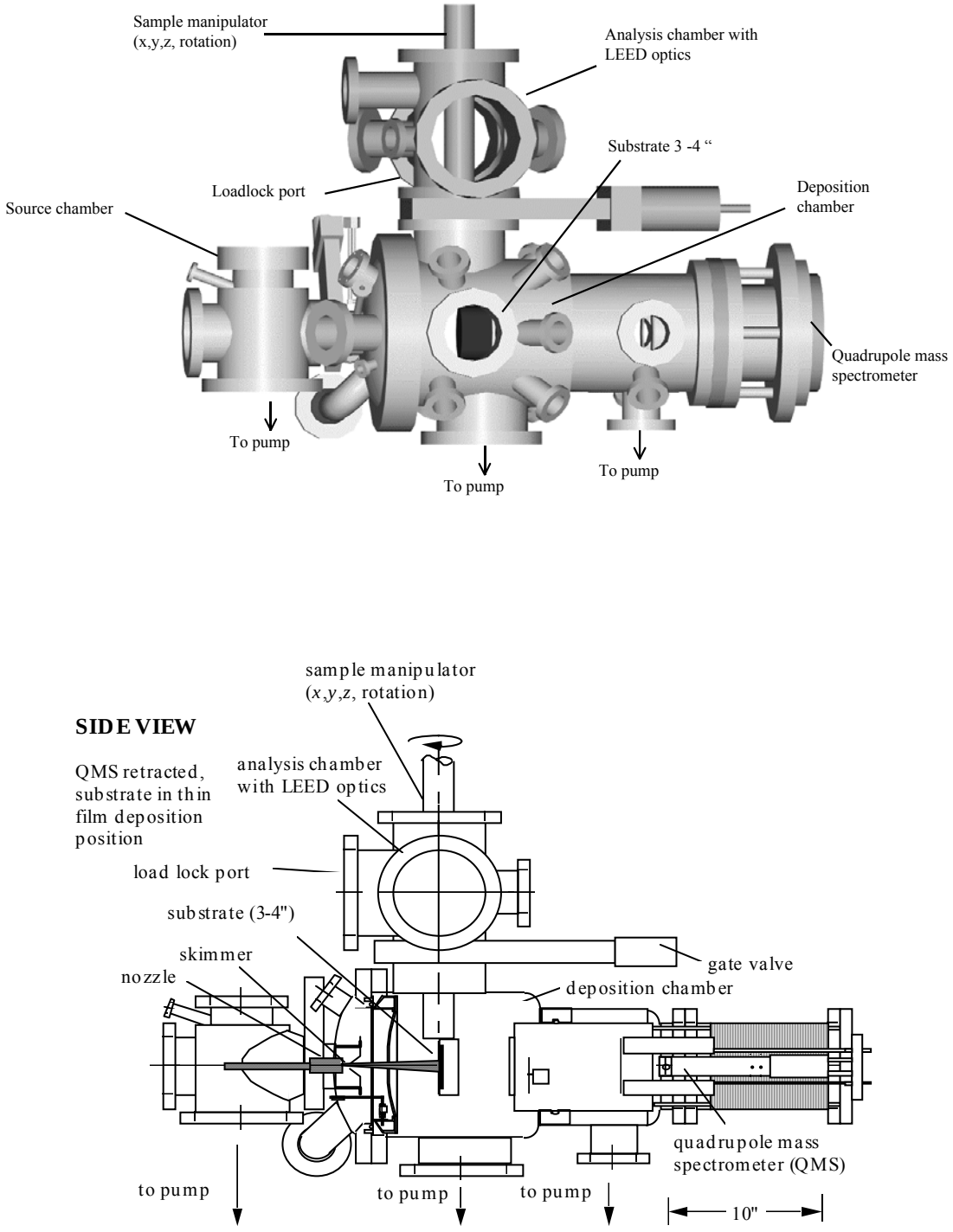

Figure 2-1 Side view of the thin film deposition chamber.

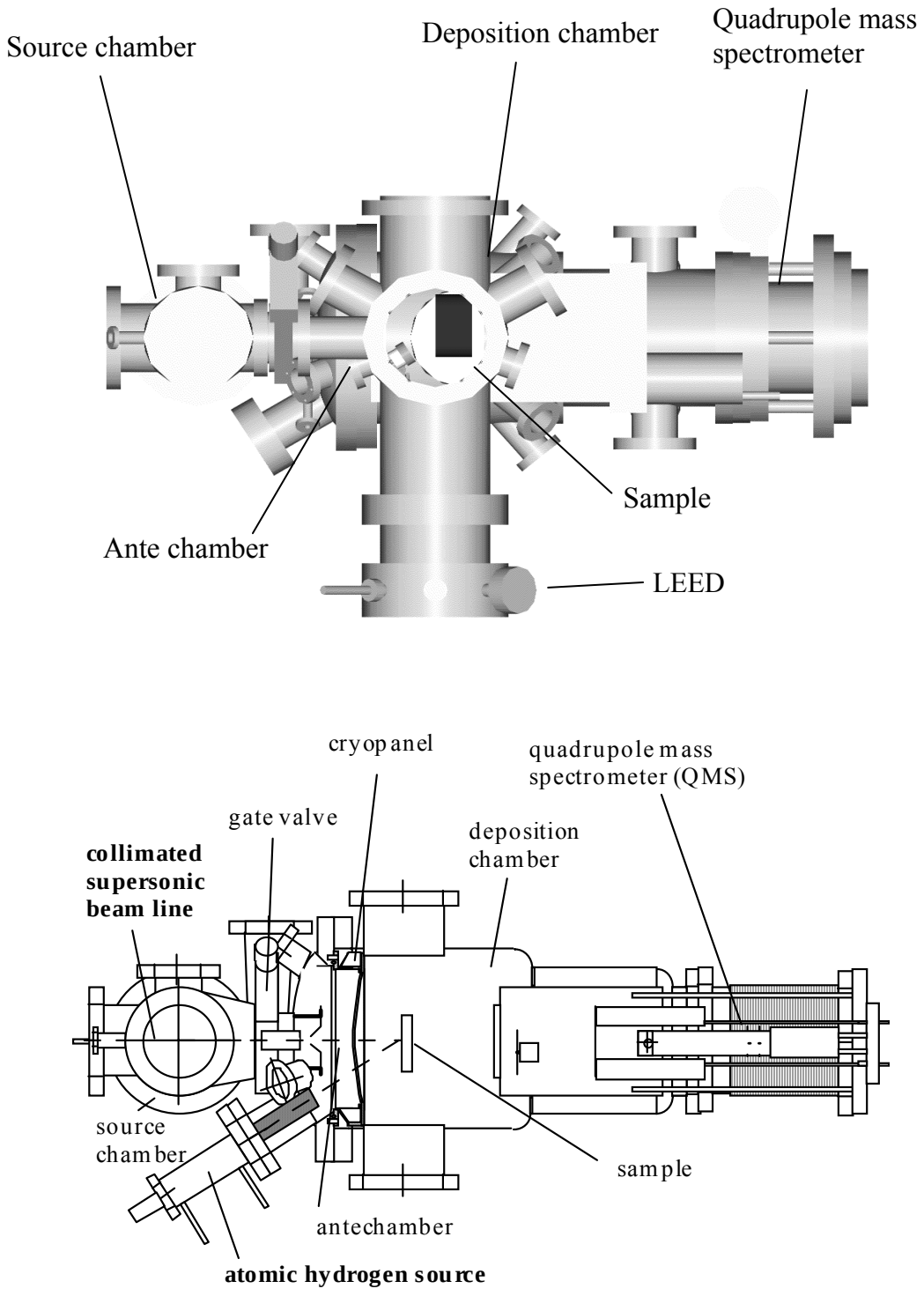

Figure 2-2 Top view of the thin film deposition chamber.

inches in diameter including specially cleaved cuts of 1 cm x 1 cm and 1.7 cm x 1.7 cm.

The source, ante, and deposition chambers of the system house the entirety of the supersonic beam from generation until beam deposition. The ante chamber employs a Pfeiffer TMU 071P tubomolecular pump pumping at 60L-s^{-1}. However, due to the nature of supersonic beam generation, the source chamber is aggressively pumped using a 520 L-s^{-1} corrosive service turbomolecular pump (Pfeiffer TMU 520C).

2.2 Generation of supersonic beam

The thin film is grown through the deposition of a supersonic molecular beam which is initiated in the source chamber. The organic of interest, which must possess a workable vapor pressure, is heated in a bubbler exterior to the source chamber. Heating the bubbler gives control over the organic's vapor pressure and hence one of the parameters in obtaining a desired flux. The evaporated material is then seeded in a carrier gas and supersonically expanded into the source chamber through a stainless steel nozzle. The nozzle was constructed out of $^1/_4$" electropolished stainless steal tube that capped on both ends with 125 μm plates containing a 150 μm aperture. Carrier gasses including He, N_2, and Ar are introduced to the bubbler using a general service mass flow controller (MKS 1179 series). The nozzle is also heated in order to both prevent sticking of the organic to its walls and to control the kinetic energy of the mixture. Both the bubbler and the nozzle which are illustrated in Figure 2-3 are heated using tungsten ribbon which is electrically insulated from the system by ceramic tubes and fastened in place by copper wire. Monitoring of their temperatures is done using k-type thermocouples. The supersonically

expanded gas mixture passes through the source chamber until it reaches the skimmer where the most collimated portion of the beam is allowed to enter the ante chamber. The skimmer is made of Ni and is conical in shape with a 1.5 mm diameter precisely machined entrance hole.

The ante chamber is the second step in creating a doubly differentially pumped system. During deposition, an annulus shaped liquid nitrogen shroud that is fixed to the shared wall of the ante chamber and the deposition chamber aids in maintaining a high vacuum pressure. Here the beam passes uninterrupted from the skimmer to an exit orifice in the plate separating the ante from the deposition chamber. The orifice helps further collimate the beam and defines its final shape before it is deposited. The deposited footprint is a 1.25 x 1.25 cm square. Upon entering the deposition chamber, the beam is subjected to analysis or flux tuning using the mass spec and finally controlled deposition experiment.

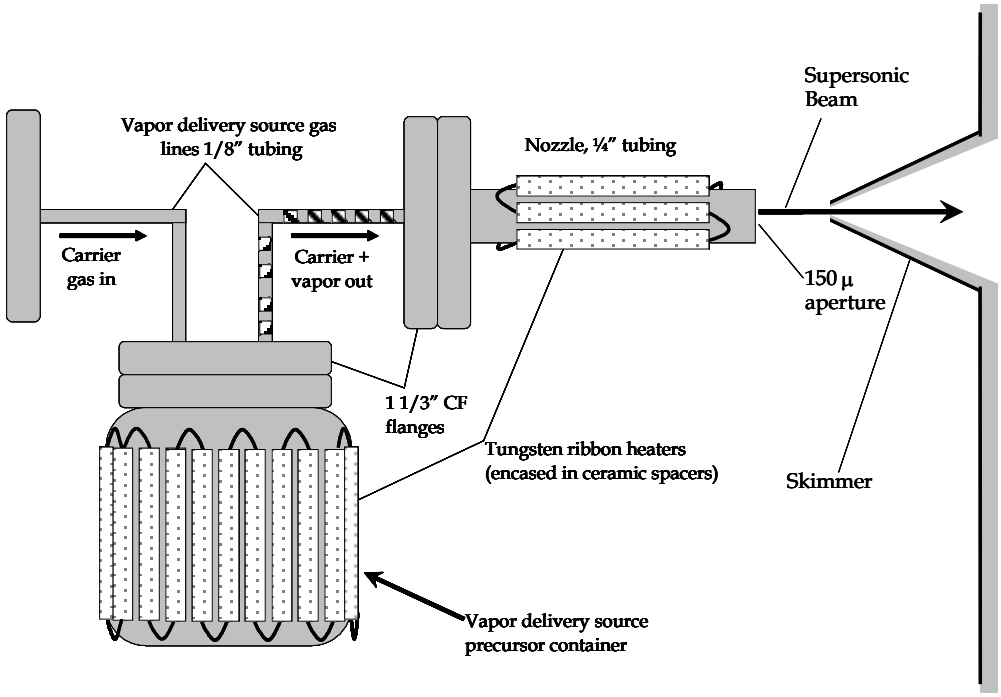

Figure 2-3 Schematic representation of supersonic beam source for low vapor pressure materials.

3 Experiments

3.1 Deposition of pentacene on OTS (Constant Beam Flux)

3.1.1 Sample preparation

3.1.1.1 Substrate cleaning

Before deposition of the SAM, the silicon Si (100) wafers (100 mm single side polished, 500-550 μm thick, doped with boron) had 300 nm of silicon dioxide (SiO_2) grown on them through a wet thermal process and are extensively cleaned using sonication and UV Ozone techniques. In the first step of the cleaning process, the wafers are submersed in a chloroform solution and sonicated for 15 min. The halogenated chloroform acts as a degreaser and removes gross organic particulates. The wafers are then remove and placed in a bath of deionized (DI) water for an additional 15 min of sonication. This helps to remove debris and any residual chloroform. Finally, a UV Ozone clean is performed in which the substrates are exposed to UV radiation for 10 min while in an oxygen rich environment. This clean acts to eliminate any remaining organic molecules through a photochemical oxidation process which converts these mainly hydrocarbons and oils into gasses and water-soluble products.

3.1.1.2 Deposition of OTS

The deposition of OTS was done through a solution based process[16]. In a glove box under N_2 environment with H_2O and O_2 content less than 1ppm, 100 mL solution of anhydrous hexadecane (>99%) and anhydrous chloroform (>99%) were mixed in a 4:1 ratio. Next, 0.1 mL of OTS was added to the solution in a volumetric flask which was repeatedly shaken for approximately

30 seconds. The solution was transferred to a Petri dish to which the cleaned substrate was added. It was then covered and allowed to sit for one hour. Following the deposition, a 30 second post-dip was performed in order to remove polymerized residue. The post-dip consisted of a 4:1 solution of hexadecane and chloroform prepared as before minus the polymerizing agent. Upon removing, the sample was allowed to dry and cleaned further by a 25 min sonication in a chloroform bath. Each of the steps were performed in immediate succession, and within 15 minutes of completing the final step, the samples were placed in the UHV chamber.

3.1.2 Beam preparation

Pentacene for all the experiments was purchased from Sigma-Aldrich Corp. (99.8%). For the actual film deposition, the substrates are loaded into the chamber through the load lock interface as previously described. Prior to substrate entering the deposition chamber, the supersonic beam was initiated and optimized. This employed the use of the mass spec. mounted in the line-of-site position where the flux could be continuously monitored during adjustment of the beam. Of particular importance is the nozzle's position relevant to the skimmer. Here, the chamber allows for x, y, and z translational adjustment of the nozzle in order to place the skimmer in the optimal position of the beam's expansion. With the nozzle and skimmer in place, the bubbler's temperature is adjusted until the desired flux is attained and shown to be stable. Finally, a shutter capable of preventing the beam from entering the deposition chamber was used to determine the beam-to-background ratio. Both the flux and the beam-to-background ratio were noted prior to deposition.

3.1.3 Terrace experiment

Through the chamber setup described above, a well defined collimated beam of supersonic molecules was created which allows many distinct advantages over other techniques such as chemical vapor deposition (CVD) or effusive beams. Foremost, may be the ability to perform multiple-exposure experiments where a single substrate is exposed to the beam in multiple areas for different increments of time. This capability is especially important for observing the evolution of film growth over time with minimal variation in substrate factors such as temperature, orientation etc. and also in the quality of the underlying SAM which is thought to be particularly delicate.

Once the beam has been optimized and stabilized, the substrate was translated into the deposition chamber where the shutter was opened and the growth could begin. During this experiment, the sample manipulator was used to move the substrate during beam exposure. The sample was translated in the z-direction perpendicular to the beam through incremental steps each of which comprising a fraction of the initial beam spot size. Separating the anti chamber from the deposition chamber, a square aperture was used which defined a 11.4 x 11.4 mm^2 footprint on the substrate. Through the translation of the sample, the films were grown containing eight different exposures with respective times of: 15 sec, 30 sec, 75 sec, 150 sec, 300 sec, 600 sec, 1200 sec, and 2400 sec. Illustrated in Figure 3-1, this gives a terrace effect showing the film's development as a function of time. To finish the growth, the shutter was closed and the sample was retracted back into the loadlock chamber. In order to check the stability of the beam, the flux intensity as well as the beam-to-background is again checked with the mass spec.

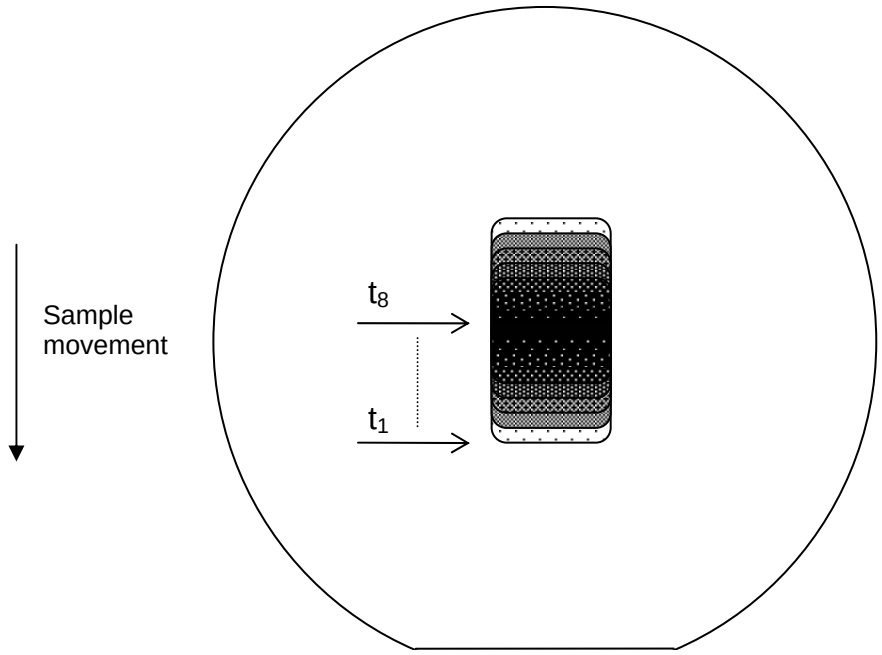

Figure 3-1 Schematic representation of the multiple exposure technique employed during thin film nucleation and growth in which 8 terraces are deposited.

When performing experiments where the impinging flux's kinetic energy is of specific interest, minimizing the influence due to random background scattering is a major concern. The doubly differentially pumped three chamber system was a key factor in achieving a high beam-to-back ground flux which was typically measure > 350:1. Also, atomic force microscopy (AFM) analysis of sample areas outside of the beam spot showed no signs of background scattering deposition.

For purposes of studying kinetic energy effects, this procedure was performed for four different energies; 1.5 eV, 2.7 eV, 4.5 eV, and 6.7 eV. For the latter three energies, helium (He) was used as the carrier gas and differences were achieved through varying the source flow rate. The 1.5 eV beam required a heavier gas, nitrogen (N_2), to be used. In order to compare the nucleation and growth characteristics of the films deposited by these beams, the incident fluxes of each were set to a constant through the adjustment of the bubbler temperature.

3.1.4 Analysis of deposited thin films and substrate

3.1.4.1 Contact angle measurements

Contact angle measurements were taken on all the substrates used in the experiment in order to determine the reproducibility of the SAM and to compare their hydrophobicities to previously recorded results on different surfaces. These measurements employed a NRL CA goniometer (Rame-Hart Inc., Mountain Lakes, NY) with an advancing droplet volume of at least 3 μL and a receding droplet volume of about 2 μm. Each sample was analyzed at four different points to ensure sample uniformity and each droplet was measured on both sides. Results are reported in the appendix 5.1.

3.1.4.2 Atomic force microscopy analysis

Following deposition, these films whose thicknesses range from submonolayer to 1000 Å thick were analyzed using a Digital Instruments Dimension 3100 scanning probe microscope (Veeco Instruments) in tapping mode. The machine's μm-precise movement easily allows for translation of the scanning head from terrace to terrace. Once positioned, surface images of 20 x 20 μm^2 size were taken from each of the eight terraces for comparison.

The issue of film growth occurring outside of the beam spot from either scattered beam or residual background was addressed by imaging a point one terrace length beyond the first terrace. In all depositions, no outside island nucleation occurred. Also, there was no visible evidence of polymerized residues of silanes being left over from the growth of the SAM. The surface appeared as smooth as the underlying SiO_2 surface which is on the order of a few angstroms.

3.1.4.3 Ellipsometry

Thickness measurements of the multilayer films were carried out using a Rudolph Auto EL – IV ellipsometer. A two-layer model was used which incorporated the underlying SiO_2 layer. Three inputs were used; a refractive index of 1.46 for SiO_2 layer, a refractive index of 1.43 for the pentacene layer, and a thickness of 3100 Å for the SiO_2. The oxide thickness was measure using the same model ellipsometer with a one-layer program.

3.1.5 Fabrication of organic thin film transistors

A four inch silicon wafer that was heavily doped n-type had 3100 Å of oxide thermally grown by wet thermal oxidation at 1100 °C. The wafer was then cleaved to obtain 4 chips of about 1.5 x 1.5 cm^2 and cleaned as before

using a sonication in chloroform, a sonication in DI water, and a UV-Ozone treatment. Also, an OTS SAM was deposited using a solution based growth technique as previously described. Each substrate was shown to be atomically smooth and free of residual polymerized silanes through AFM imaging of the surface. The treated substrates were immediately transferred to the UHV chamber and pumped done overnight to a base pressure of ~ 2 x 10^{-9} torr. The substrates then underwent a 40 min deposition in which 400 Å of pentacene was supersonically deposited at normal incidence, each with a different beam energy; 1.5 eV, 2.7 eV, 4.5 eV, and 6.7 eV.

Devices were then fabricated using gold top contacts as diagramed below, Figure 3-2. Here, a shadow mask was used to deposit the source and drain contacts under high vacuum (10^{-6} torr) and at room temperature. Through the shadow mask, a 3 x 9 array of devices was deposited directly on top of the pentacene from a thermal sublimation source. The gold contacts were deposited at a rate of 4 Å-s^{-1} to a thickness of 250 Å. The array was laid out such that each row containing 9 devices had one of three channel lengths; 31.25, 75, and 125 μm. The samples were then transferred to a four point probe station, put under vacuum (10^{-6} torr), and their field-effect mobilities, μ_{FE}, were tested in the saturation regime.

3.2 Deposition of pentacene on Si/SiO_2 (Constant Growth Rate)

3.2.1 Camber setup (G-line System)

For the following experiments, the bubbler/nozzle stage was removed from the previously described deposition chamber and mounted in a newly purchased vacuum chamber, G-line. Illustrated in Figure 3-3 and Figure 3-4 and described in-depth elsewhere[17], the setup and dimensions of the new chamber

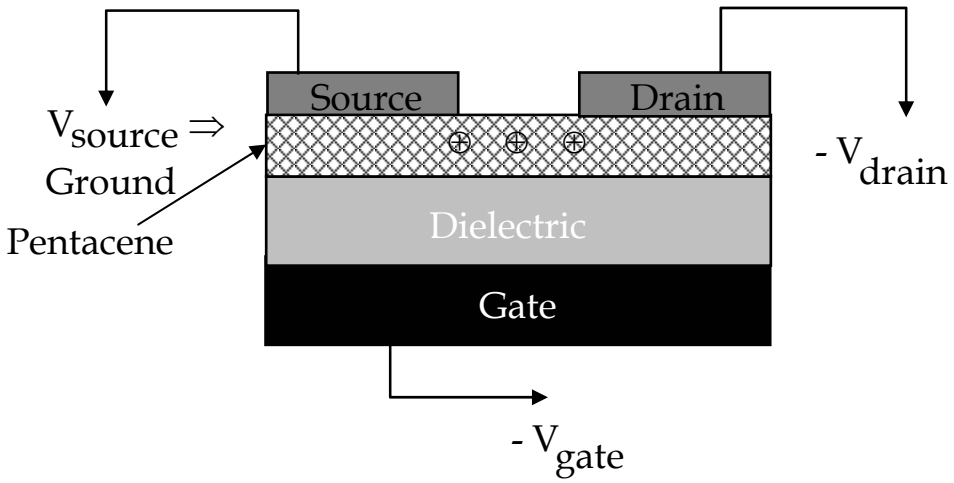

Figure 3-2 Top contact configuration for organic thin film transistors (OTFTs) fabricated using semiconducting films.

are very similar to the work previously discussed. A key factor in creating a collimated and uniform beam is the relative distances between the nozzle, skimmer, and substrate. Due to the slightly different geometry of this chamber, a skimmer with a 200 μm aperture was used. The square beam defining aperture separating the anti chamber from the deposition chamber created a well-defined beam footprint that was 9.2 mm x 9.2 mm square. From ellipsometric measurements, the beam spot's uniformity was shown to have a +/- 5 Å variance in film thickness moving from the center of the square to the corner after a 600 Å deposition.

3.2.2 Sample prep.

Samples in these experiments consists of 1" x 1" square pieces of Si(100) all of which were cleaved from the same 4" wafer. Prior to cleaving, the 4" wafer had 335 nm of SiO_2 thermally grown using a MOS furnace at CNF. The oxide thickness of each individual square was confirmed to be within 1 nm using the Filmetrics Film Measurement System in CNF. The clean which included a chloroform sonication, a DI water sonication and a UV/Ozone treatment as was previously described in sect. 3.1.1.1. Immediately following the UV/Ozone treatment the sample is transported in fluoroware to the UHV lab and put under vacuum. Estimated time of exposure to atmosphere was 30 min. In every case, samples were prepared in the evening which allowed for the UHV chamber to pump down overnight. Depositions were performed the following day with an initial base pressure around $5x10^{-9}$ torr.

3.2.3 Constant growth rate calibration

Due to the geometry of the vacuum chamber, experiments under constant growth rate conditions were predicted to be most fruitful. In order to replicate

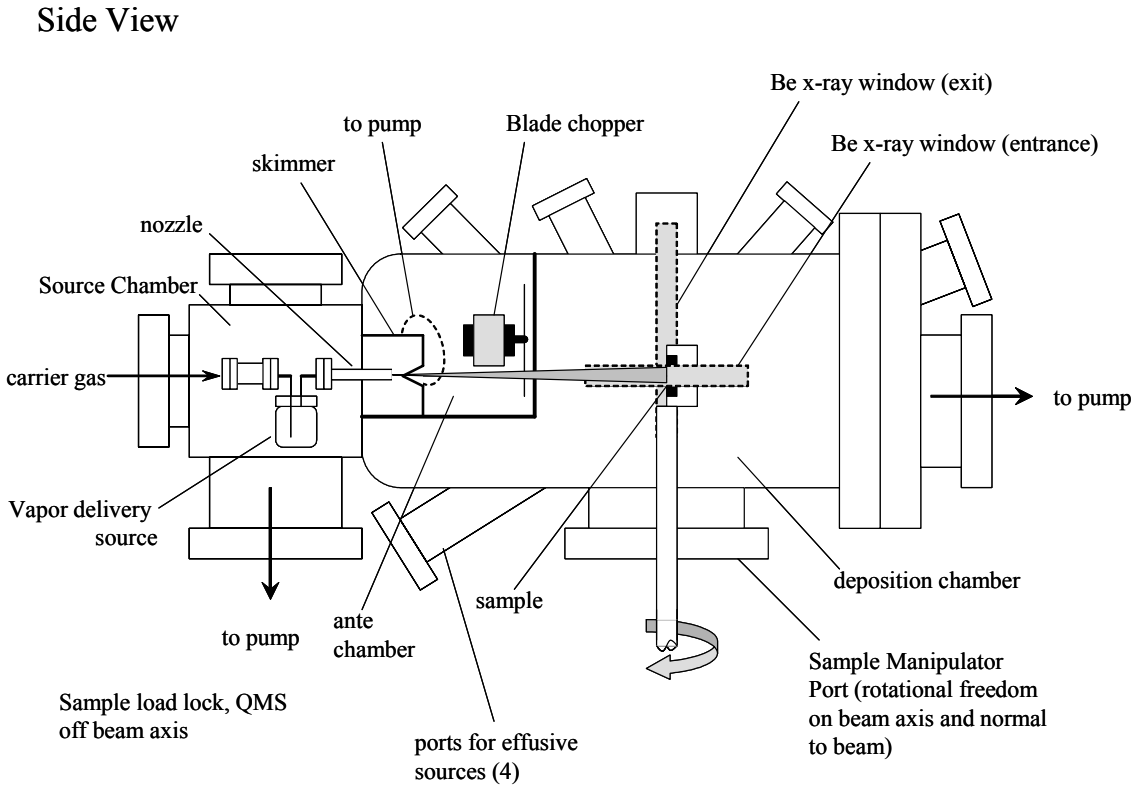

Figure 3-3 Side view schematic drawing of the gas source deposition system (G-Line system).

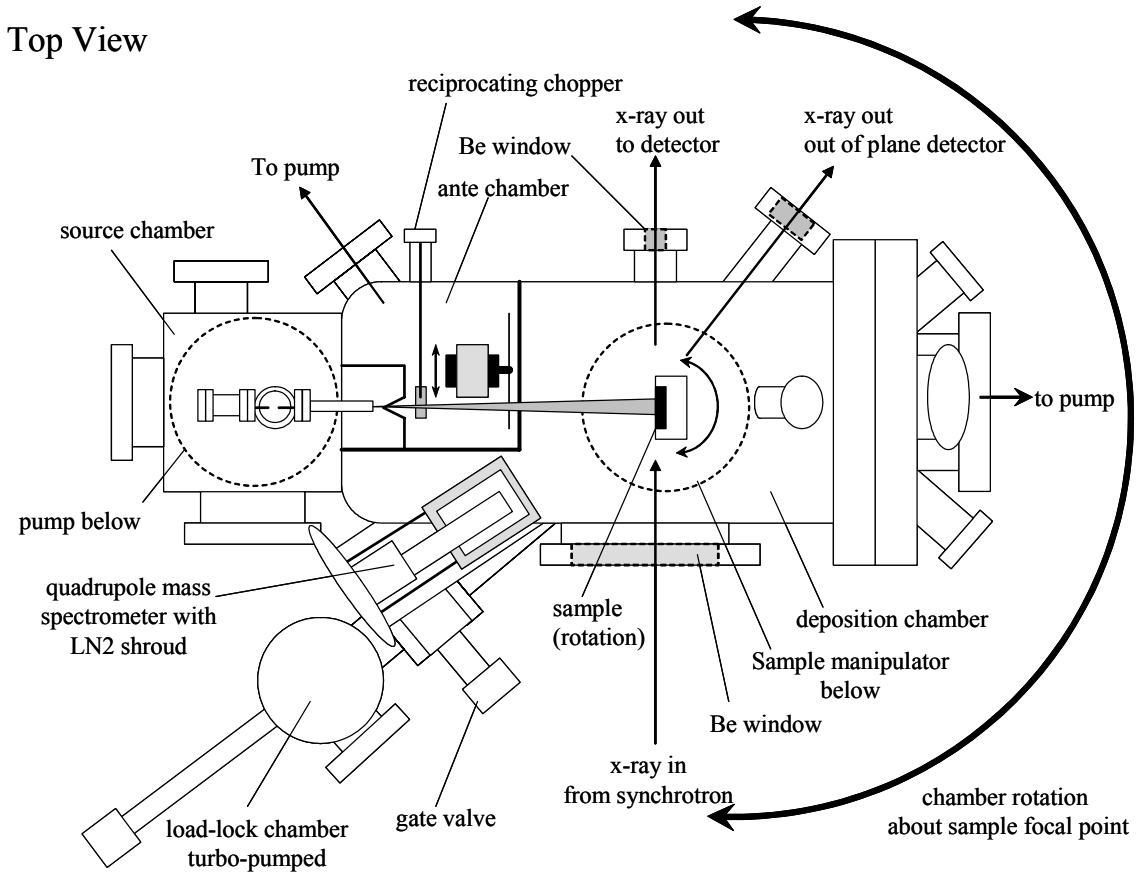

Figure 3-4 Top view schematic drawing of the gas source deposition system (G-Line system).

these conditions under the demands of the different beams, calibration runs were made varying the bubbler temperature and therefore the flux of pentacene impacting the substrate. A series of three depositions per beam energy were conducted for a single exposure time. Variations in run conditions were minimized by depositing each of the three films on a single substrate. Thickness analysis of the films, which was done by ellipsometry and will be described in the results section, allowed for the calculation of film growth rate as a function of bubbler temperature. Data plots and numerical fits are presented in Appendix 5.2.

3.2.4 Experiment (constant growth rate)

For these experiments, the previous calibrations were used to determine the appropriate bubbler temperatures that produce a growth rate of 15 Å/min for each beam energy. Three beam energies were used; 2.7 eV, 4.5 eV, and 6.7 eV.

In each experiment, the bubbler was slowly heated to the deposition temperature over a period of 3-4 hours where it was held for an additional hour to stabilize any gradients. The shutter was then opened and the substrate was exposed to the beam. During the exposure, the substrate was moved seven times perpendicular to the beam. The distance of each move was $1/8^{th}$ the total length of the beam's footprint. The eight terraces created from this had deposition times of 1.25, 2.5, 5, 10, 20, 40, 80, and 160 minutes.

3.2.5 Analysis of deposited thin films and substrate

Topological surface images were again taken using a Digital Instruments Dimension 3100 AFM and analyzed using Nanoscope (v 5.0). Ellipsometric measurements were taken as previously described using the Rudolph Auto EL –

IV ellipsometer. All terraces had multiple layers and were able to be analyzed using the ellipsometer's two-layer model.

4 Results and Discussion

4.1 Effects of OTS treatment on pentacene growth

4.1.1 Smoothening effect

A Digital Instruments 3100 AFM was used to obtain topological surface information from pentacene films that were deposited supersonically onto silicon dioxide surfaces treated with octadecyltrichlorosilane (OTS). The information has been analyzed using Nanoscope (v 5.0) software. All images were initially subjected to a second order plane fit prior to data extraction.

Modeling the roughness evolution of a film with deposition time or possibly film thickness gives a first look into the mechanics that underlay film growth. In doing so, the Nanoscope software was used to calculate root-mean-square (RMS) roughness. This is plotted against the films deposition time in Figure 4-1.

This plot compares the roughness evolution for each of the four energies. As can be seen from the graph, a clear dependence on incident beam energy is not apparent. An interesting effect, however, is the second minimum in RMS roughness that is observed somewhere between 300 and 1500 seconds. This "smoothening effect" is observed in each energy series that was deposited. The minimum is a stark contrast to the roughness evolution observed on untreated

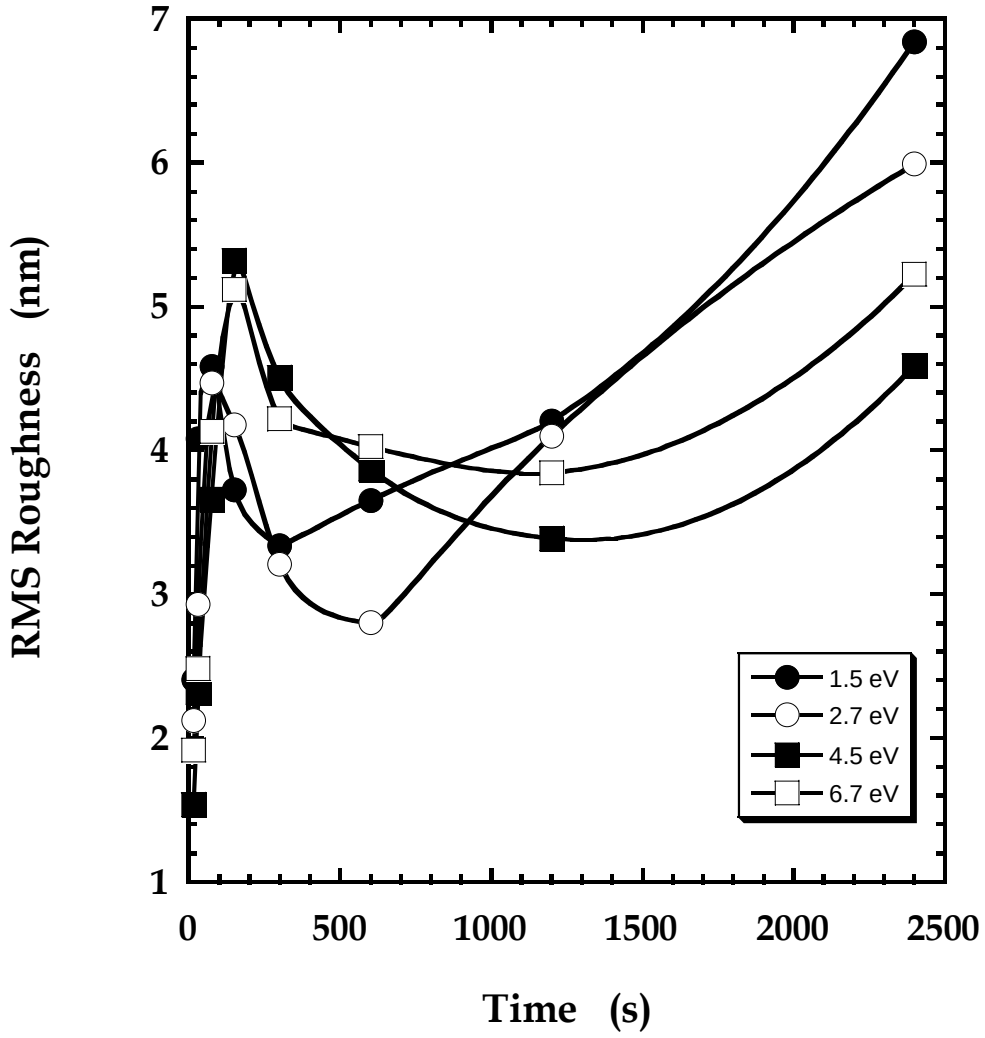

Figure 4-1 Root mean spuare (RMS) roughness as a function of film deposition time for four incident kinetic energies at normal incidence.

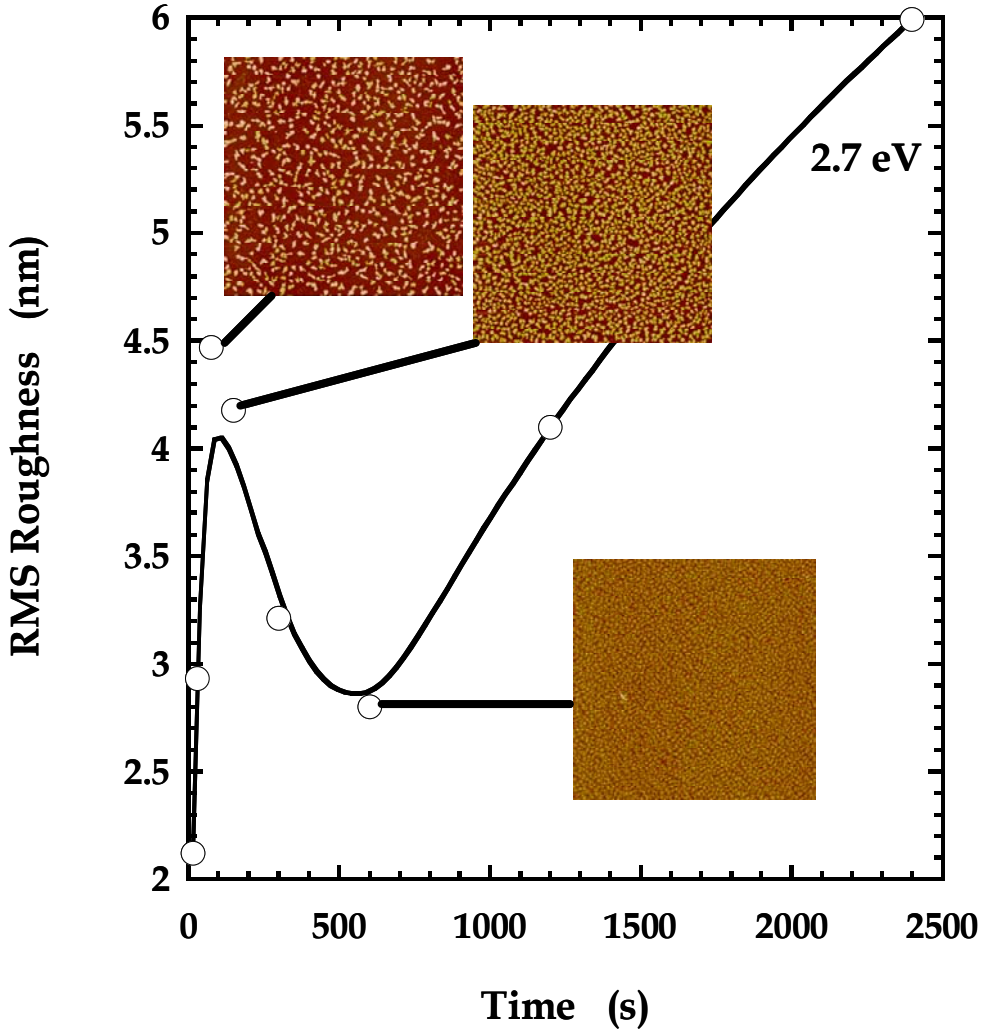

Figure 4-2 Illistration showing the correlation between "Smoothening Effect" and substrate closeout.

SiO_2, where the roughness would scale with a simple power law fit relative to its thickness.

Matching the AFM images with their appropriate positions on the roughness vs. deposition time curve illustrates that this smoothening effect coincides with the closeout of the substrate, Figure 4-2. It is arguable that this minimum in roughness marks a transition in growth mechanics and a look at the film's evolution on either side of the minimum may provide some insight.

4.1.1.1 Film evolution prior to roughness minimum

To further investigate this smoothening effect, Figure 4-3 shows some of the AFM images of a single terrace experiment at the incident beam energy of 2.7 eV. The images depict a very three dimensional growth mechanism which initiates soon after the formation of long flat-lying islands. These islands appear almost immediately and are short lived. Histogram analysis of the first three terraces (15 s, 30 s, 75 s) shows that most of the flat-lying islands are two monolayers thick in each of the terraces, ~ 2.85 nm. That is, they do not seem to grow thicker. Actually, the islands appear to be shrinking in top surface area. In Figure 4-4, histograms of the first three islands are presented.

With the onset of three dimensional growth, the flat-lying islands quickly disappear and very abrupt needlelike islands begin to appear. Without completing the first monolayer, these islands appear to grow with strict Volmer-Weber growth. Also, they don't seem to coalesce. Line scans of the AFM images were taken and are shown in Figure 4-4. The line scans confirm a needlelike island formation protruding vertically from the substrate surface.

Two interesting observations can easily be made from this analysis; the first of which is that no lateral growth is apparent from nucleation until the

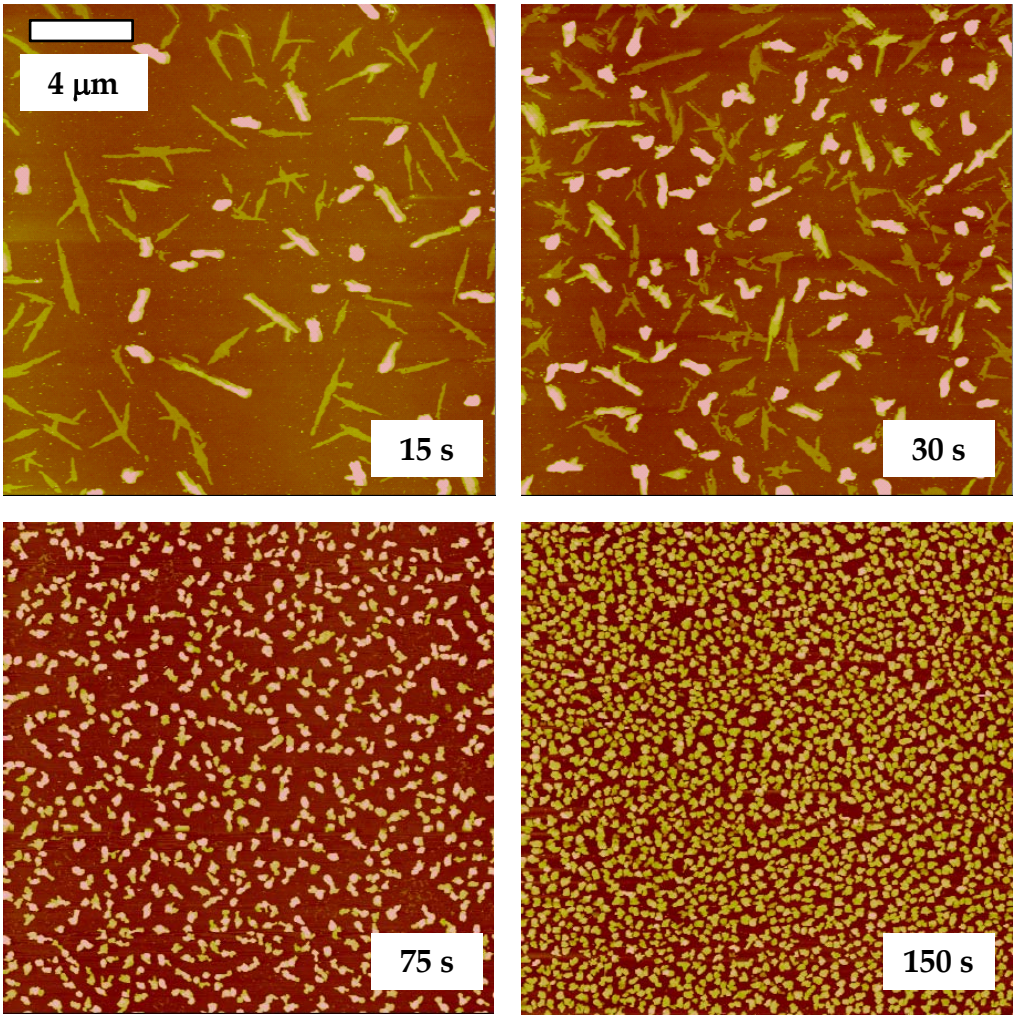

Figure 4-3 Atomic force microscopy (AFM) images of the 2.7 eV beam used to deposit pentacene on OTS.

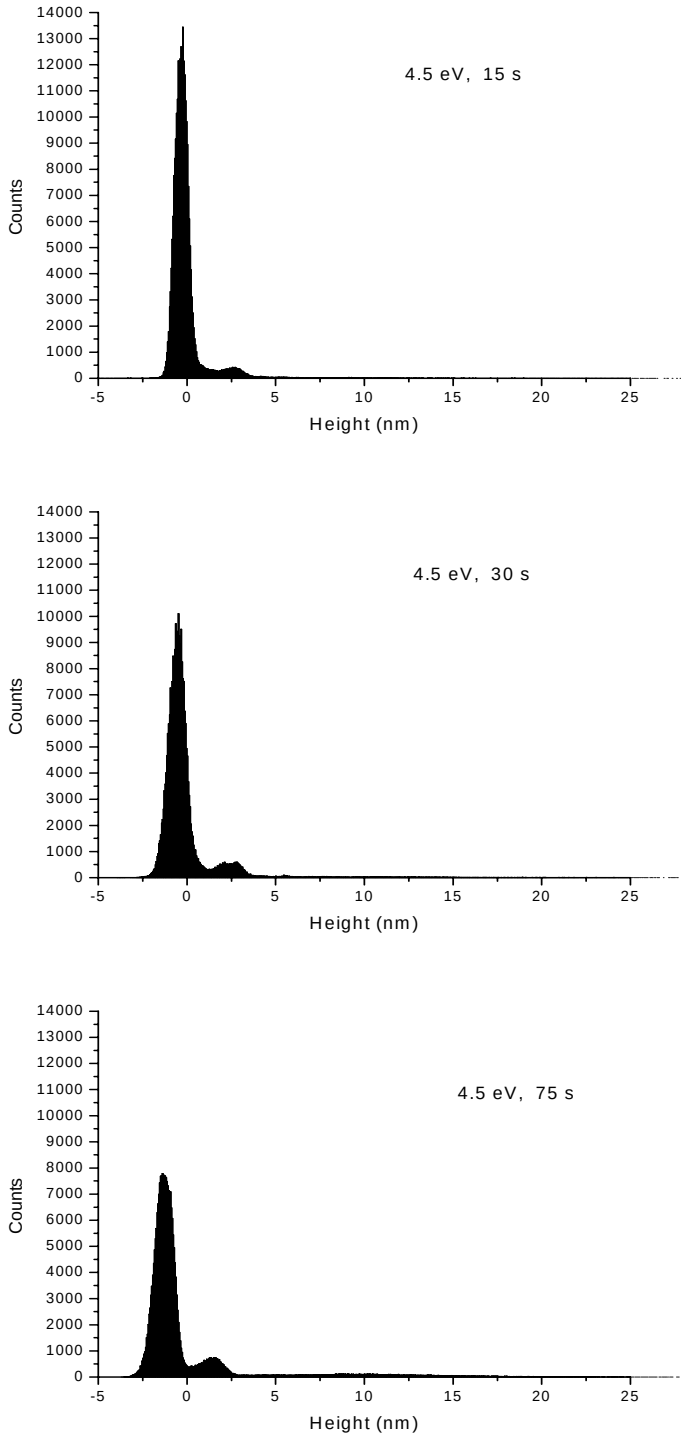

Figure 4-4 Histogram analysis shows increase in coverage of broad 2D islands.

substrate is covered. This is clearly visible from the line scans where the needlelike islands multiply rather than grow. Secondly, the islands tend to grow quickly until a saturation height is reached and stop. Quickly is to say that the timescale with which the experiments were carried out (15, 30, 75, and 150 s) captures few islands in mid-growth. This halting of growth is evident when comparing the line scans from different points of time. Typically, four terraces were grown with an exponentially increasing time of deposition. The needlelike islands appear in the first terrace and begin to percolate by the fourth. Through each of these images, the vast majority of islands remain 10-12 nm high. That is to say the islands that exist in the first couple images do not appear to have grown by the time that the last couple images were captured. This growth regime can be summarized by the growth of needlelike islands that seem to reach a "characteristic height" and than halt.

4.1.1.2 Film evolution subsequent to roughness minimum

From the point of substrate closeout onwards, film growth is effectively a homogenous process. The timescale which this experiment was run focuses on the transition from pre to post growth mechanics and does not capture sufficient growth of the latter to give a complete picture of what is happening. Running this experimental setup again with the deposition time series adjusted to capture more progressed film growth is necessary for a more thorough analysis.

4.1.1.3 Theory on film growth prior to substrate closeout

A possible explanation for the smoothening effect just described is that the OTS treated surface which was shown to be extremely hydrophobic creates an interface with pentacene that has a much higher surface energy than is

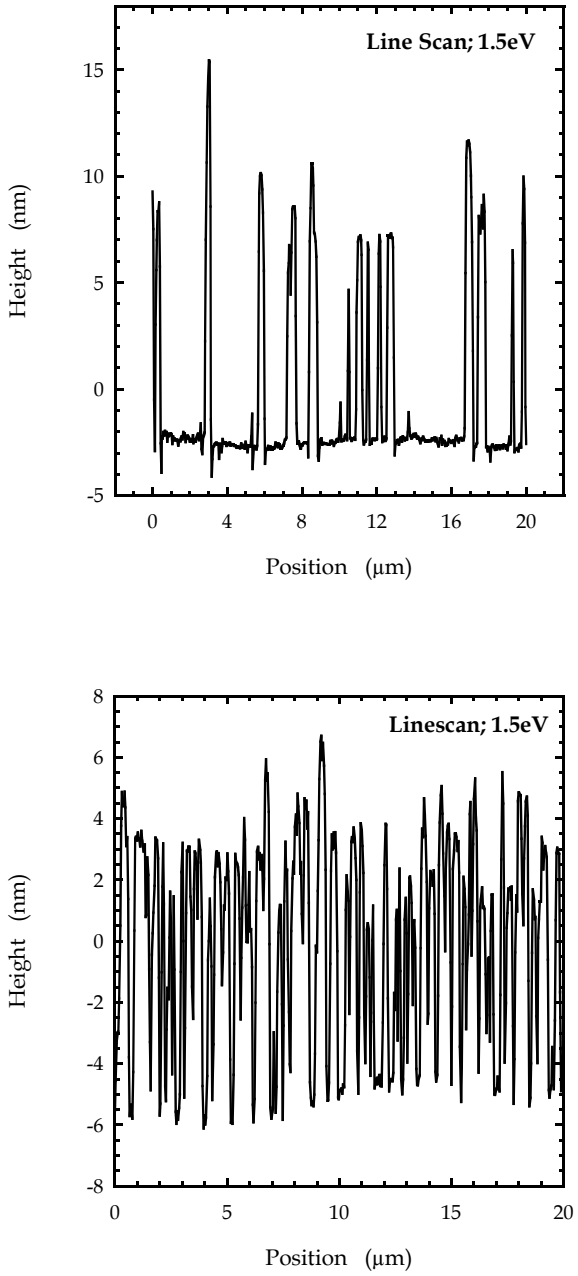

Figure 4-5 Line scans taken from AFM analysis show an increase in the number of islands but no growth beyond a "characteristic height"

observed on an SiO_2 surface. This makes spontaneous island nucleation unlikely. Also, the broad 2D islands that appear almost immediately are most likely due to nucleation on surface defects and in a metastable state. Describing them as metastable is believable when considering how quickly they disappear once three-dimensional growth commences.

The initial growth mechanism underlying the appearance of needlelike islands and rapid roughening stems from two sources; growth from impinging flux and vertical diffusion of the broad 2D islands. As shown in Figure 4-3, the broad 2D islands appear to shrink as they advance three dimensionally. This 3D growth is however not endless and seems to be stunted not by diffusion limitations but rather by a thermodynamic equilibrium. This argument is made in an attempt to explain the "characteristic height" reached by the needlelike islands. Had diffusion factors been in play, the appearance of a characteristic height would never have occurred and broad array of islands would be present with their heights being a function of their relevant nucleation times.

A thermodynamic equilibrium provides an explanation for the characteristic height and the rapid roughening that occurs. Equation 4-1 models the Gibbs free energy of an interface with V and A being volume and area, γ being surface energy, PS denoting the pentacene-substrate interface, and PV denoting the pentacene-vacuum interface.

$$G_{system} = (G_{Bulk} * V_{Bulk}) + (\gamma_{PS} * A_{PS}) + (\gamma_{PV} * A_{PV})$$

Equation 4-1

The equilibrium is reached when the Gibbs free energy is at its minimum. In this effort, two opposing forces are produced; the reduction of

island-substrate surface energy from the upward diffusion of pentacene and the creation of island-vacuum surface energy through vertical island growth. Under this growth theory, a characteristic island height would be expected once these two forces balance. The drive for vertical island growth on OTS treated surfaces may also be expected when considering how the hydrophobisity of the OTS molecule would effect the surface energy, γ_{PS}, of the substrate. The argued thermodynamic equilibrium also explains the observed smoothening effect. Once the equilibrium is reached vertical progression and hence roughening would stop. In fact, as more needlelike islands are formed and the film fills in, roughness should go down as is observed. Without this equilibrium, growth would have continued and also roughening. Of course a transition in growth mechanisms would explain a change in rates of roughening, but not a minimum. Additional experiments would help confirm this theory. In particular, lowering the temperature of the substrate during film deposition could change the island heights from being thermodynamically limited to diffusion limited. An array of island heights should appear confirming the equilibrium theory.

4.1.2 Power spectral density

4.1.3 Organic transistors

The deposition of a SAM prior to the growth of the semiconductor provides an excellent way to study the film's growth dependence on the surface-molecule interaction. The growth at this interface is extremely important as it is in this region where the crystalline structure almost entirely determines the films electrical properties. It is widely known that the crystal ordering process can be greatly affected and perhaps the electrical properties enhanced by altering the incident kinetic energy of the impinging beam.

The mobility, μ, can be described as the ease at which electrons flow through the film. For a film composed of multiple grains, the mobility can be broken into the charge transport through the bulk of the grain, μ_g, and across grain boundaries, μ_b. These two contribute to the overall mobility as:

$$\frac{1}{\mu} = \frac{1}{\mu_g} + \frac{1}{\mu_b}$$

Equation 4-2

To date, much work[18,19] has been done that shows that improvements to film mobilities can be made by increasing the size of the grains in the lateral direction. This implies that the limiting factor for typical device performance is the mobility across the grain boundaries, $\mu_g >> \mu_b$.

Organic thin film transistors (OTFTs) were fabricated by supersonically depositing pentacene at four different energies on Si (100) wafers. The wafers had 3100 Å of thermal oxide grown on them as well as single atomic monolayer (SAM) of OTS. Gold top contacts were thermally sublimated under vacuum conditions (10^{-6} torr) with three different channel lengths and the devices electrical properties were tested using a 4-point probe station, again under vacuum conditions (10^{-6} torr). A detailed procedure is described in section 3.1.5.

AFMs images of these films at the four different energies were taken and a comparison between pentacene growth on OTS and previous work that was done on Si/SiO_2 is shown in Figure 4-6. Initial thoughts after the AFM inspection were that the drastically smaller grains that were produced by the OTS treatment would greatly increase the number of charge trapping grain

boundaries between the device's contacts and therefore decrease the overall mobility of the device.

Mobilities from these devices were extracted from the saturation regime and are presented in Figure 4-7. A strong relationship between incident kinetic energy of the beam and the mobility is easily seen. An interesting result, however, is that the small mobilities predicted by the small grain structure of the film did not occur. To the contrary, the mobilities attained by these devices reached as high as .6467 $cm^2–V^{–1}–s^{–1}$ which is a significant increase to the previous work done on thermally grown SiO_2 shown in Table 4-1. Also to note is that at each energy, the mobility of the device increased with decreasing channel length. The smaller channel lengths at this size regime would of course decrease the number of grain boundaries between contacts and in turn increase the mobility.

It appears as though the OTS treatment is creating two competing effects to the mobility; an expected decrease due to a much larger number of grain boundaries and a dominating increase of an unknown origin. An argument can be made to the presumed assumption of $\mu_g >> \mu_b$ that in fact the contributing factor to the overall mobility from the bulk grain (μ_g^{-1}) is on the same order as that from the grain boundary (μ_b^{-1}). If the presumed assumption was correct, any increase in μ_g stemming from surface modification would have a negligible effect on the overall mobility.

4.2 Pentacene deposition at constant growth rate

Thin films of pentacene have been deposited at a constant growth rate (15 Å-min^{-1}) onto Si(100) wafers with 3350 Å of thermal oxide grown on them. The pentacene was deposited under supersonic beam conditions and at 3

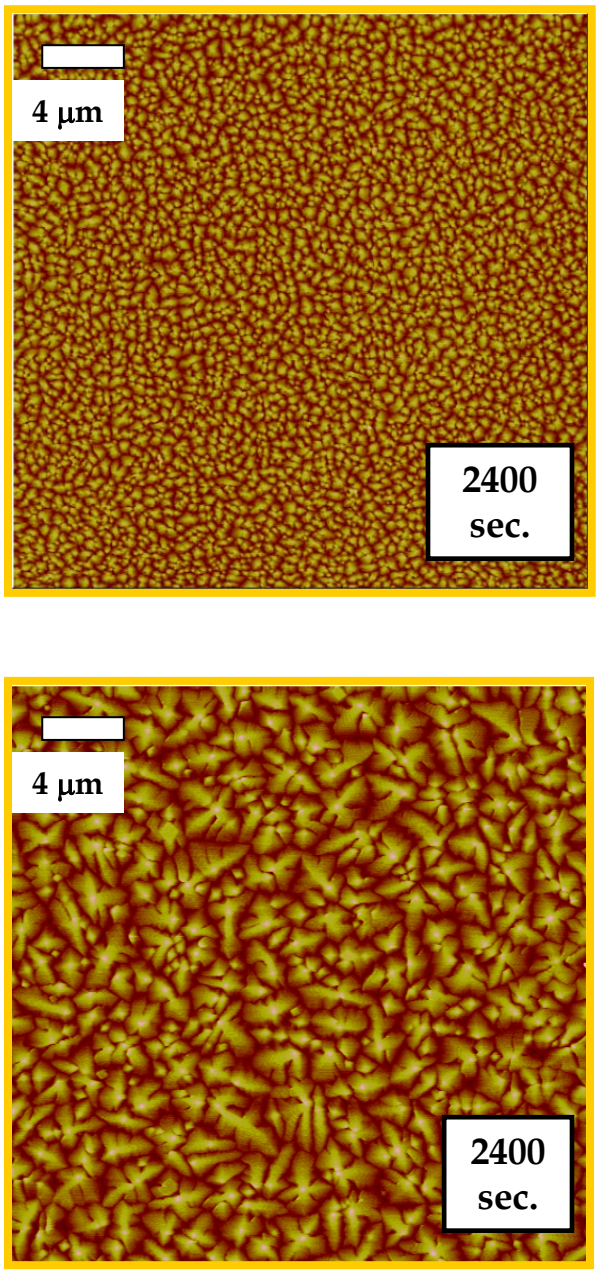

Figure 4-6 OTS treatment of a surface (top) produces compact islands of similar shape but with drastically smaller grain size than previous work done on untreated Si/SiO_2[16] (bottom).

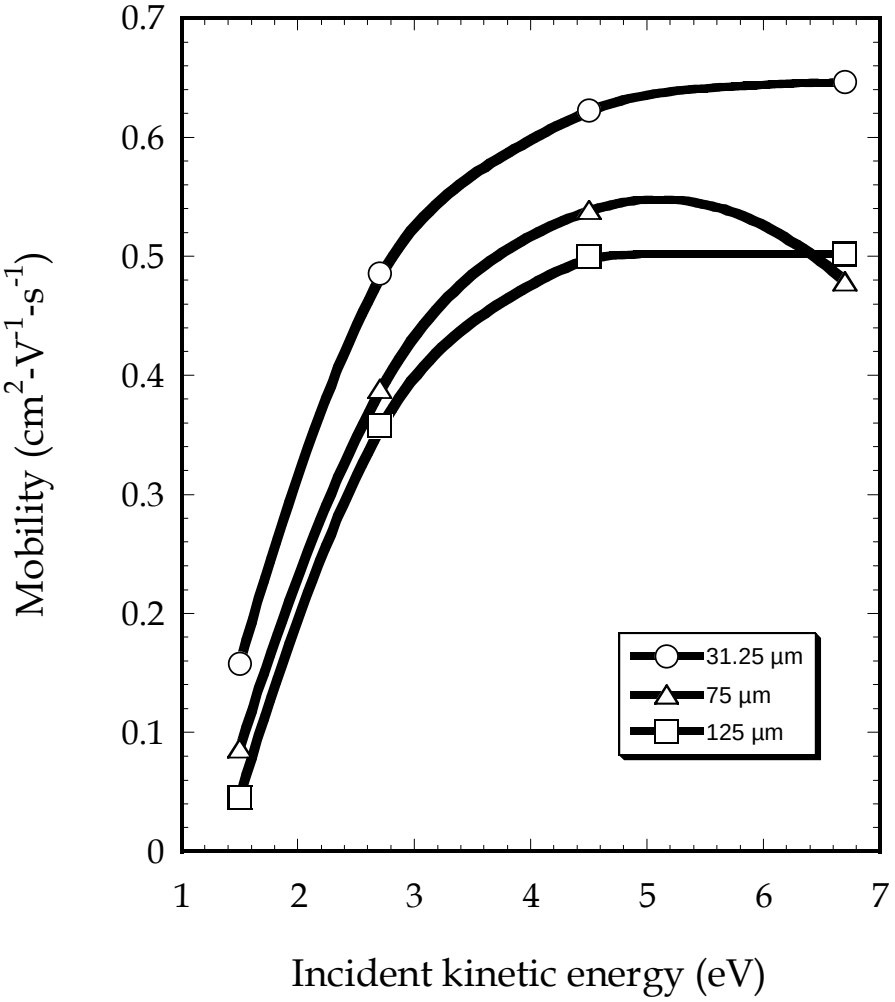

Figure 4-7 Mobility results from devices made using three different incident kinetic energies and with three different channel lengths.

Table 4-1 Mobilities attained through the surface treatment with OTS have significantly higher device performance than device results produced on untreated thermal oxide **[16]**.

Substrate	**Mobility (μ) (cm^2-V^{-1}-s^{-1})**
SiO_2	.27
SiO_2 modified with OTS	.6467

different incident energies (2.7 eV, 4.5 eV, and 6.7 eV). An initial series of runs was performed for the purpose of calibrating beam fluxes to attain constant growth rate conditions. Flux calibrations are reported in the Appendix 5.2 and a detailed experimental setup is provided in Section 3.2.3.

Using the program Nanoscope v 5.0, an analysis of the AFMs taken from all of the terraces deposited through the runs allowed for the calculation of the one-dimensional power spectral density (1D PSD) for each. 1D PSD has proven to be a useful tool in characterizing film development in particular the morphological surface changes that occur throughout a deposition. Key factors that were looked at in this analysis include the roughening exponent (α), the growth exponent (β), and the correlation length (ξ).

In hopes of calculating meaningful exponents that are indicative of a single growth mechanism, AFMs of films that have already progressed to the multilayer regime were analyzed and compared. In extracting the roughening exponent from the AFM, the self-affine region of the 1DPSD was plotted against its spatial frequency and fitted with a power law. The roughening exponent was then calculated from the exponent of the power law fit and averaged with the other AFMs from the deposition. This calculation and the resulting α's are shown Figure 4-8.

The growth exponent, β, has been calculated for the supersonic deposition of pentacene at three incident energies; 2.7 eV, 4.5 eV, and 6.7 eV. RMS roughness of each of the films was plotted against film thicknesses obtained from ellipsometric measurements. The growth exponent is determined from the slope of the power law fit as shown in Figure 4-9.

The lateral correlation length, ξ, as described earlier has been calculated again through inspection of the AFM image. Here, the 1D PSD is plotted

Figure 4-8 The 1D PSD attained from AFM analysis is used in calculating the roughness exponent (α). Figure 4-8a showes the self-affine portion of the 1D PSD which is plotted against its spatial frequency and fitted with a power law. In Figure 4-8c, the roughness exponent is plotted vs. the four incident kinetic energies that were used.

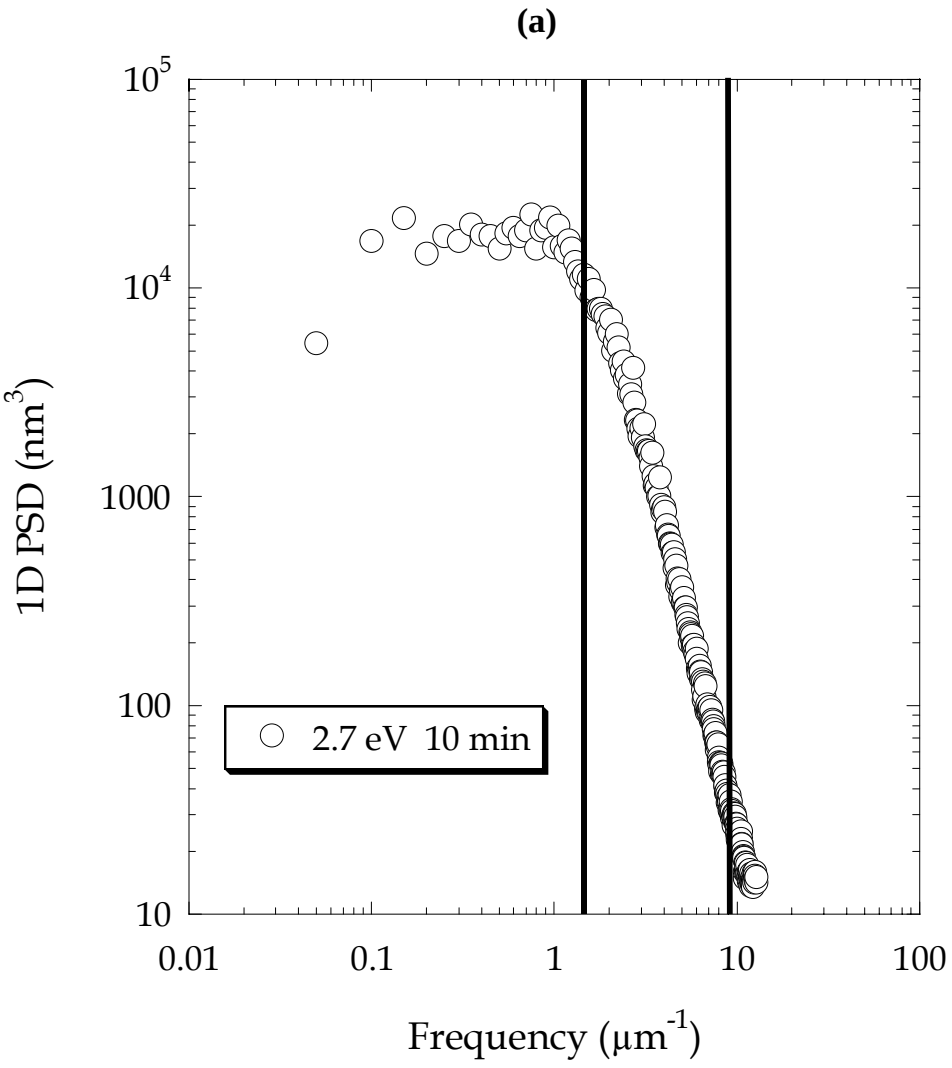
(a)
10^5
10^4
1000
100
10
1D PSD (nm^3)
2.7 eV 10 min
0.01
0.1
1
10
100
Frequency (μm^{-1})

Figure 4-8 (continued)

(b)

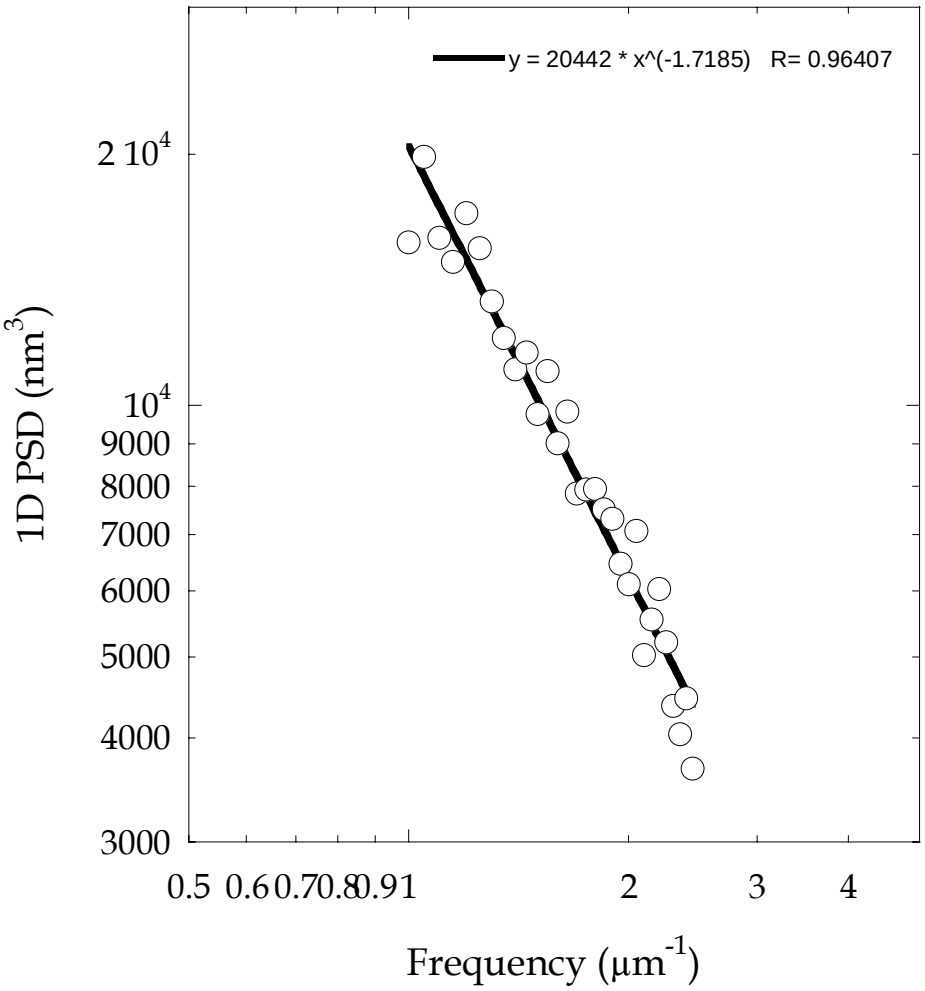

Figure 4-8 (continued)

(c)

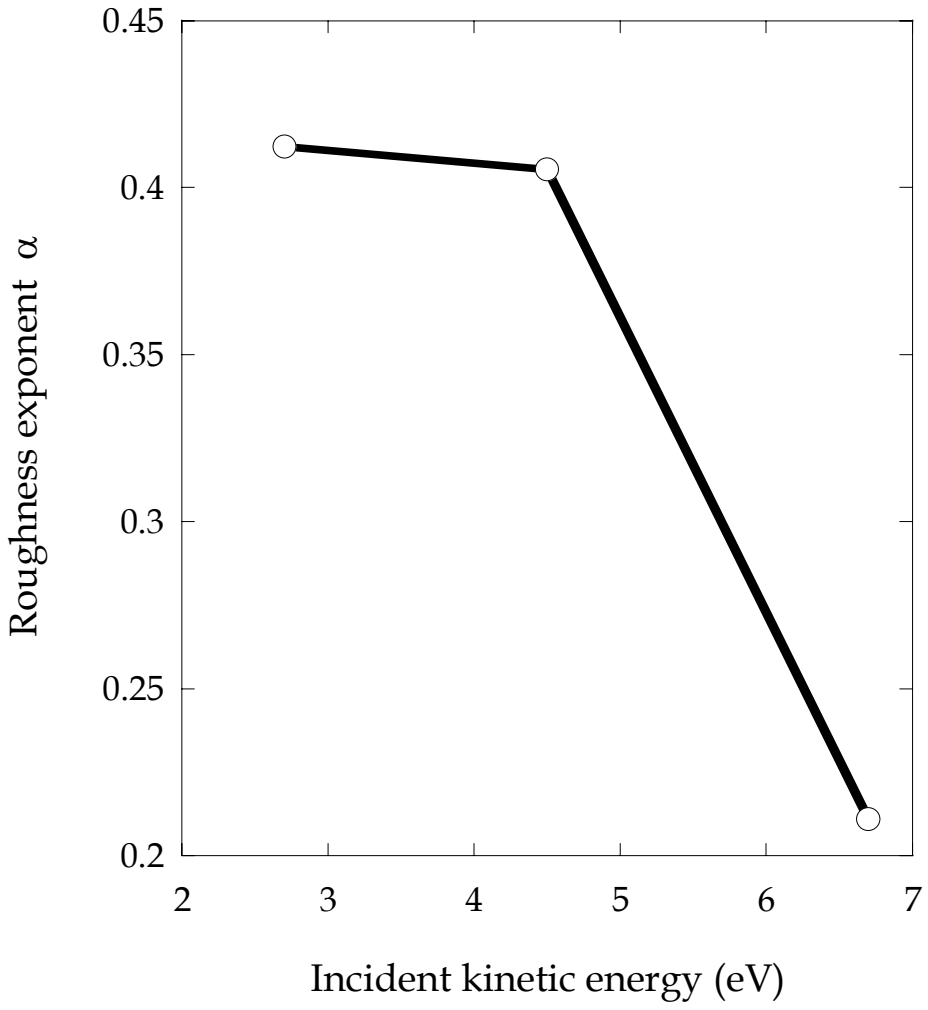

against its spatial frequency. The correlation length is defined as the inverse of the spatial frequency that separates the self-affine region (the negatively sloped portion) from the frequency independent region (the horizontal portion). Since the flux of the deposition beam was calibrated to constant growth rate (~ 15 Å-min^{-1}), the correlation length can be related to film thickness as a function of deposition time. Figure 4-11 shows that after the film thickness reaches ~ 250 Å, the correlation length remains about constant and can be averaged for all multilayer images. Correlation length as it relates to incident beam energy is pictured in Figure 4-12.

From the data presented, a strong relationship between the film's correlation length and incident kinetic energy is not apparent. The correlation lengths are very similar to the groups results carried out on the thin film deposition chamber **[16]**. These results were from the first set of terrace experiments performed the supersonic gas source deposition chamber for organic semiconductors and more data will need to be collected in order to give a more complete picture.

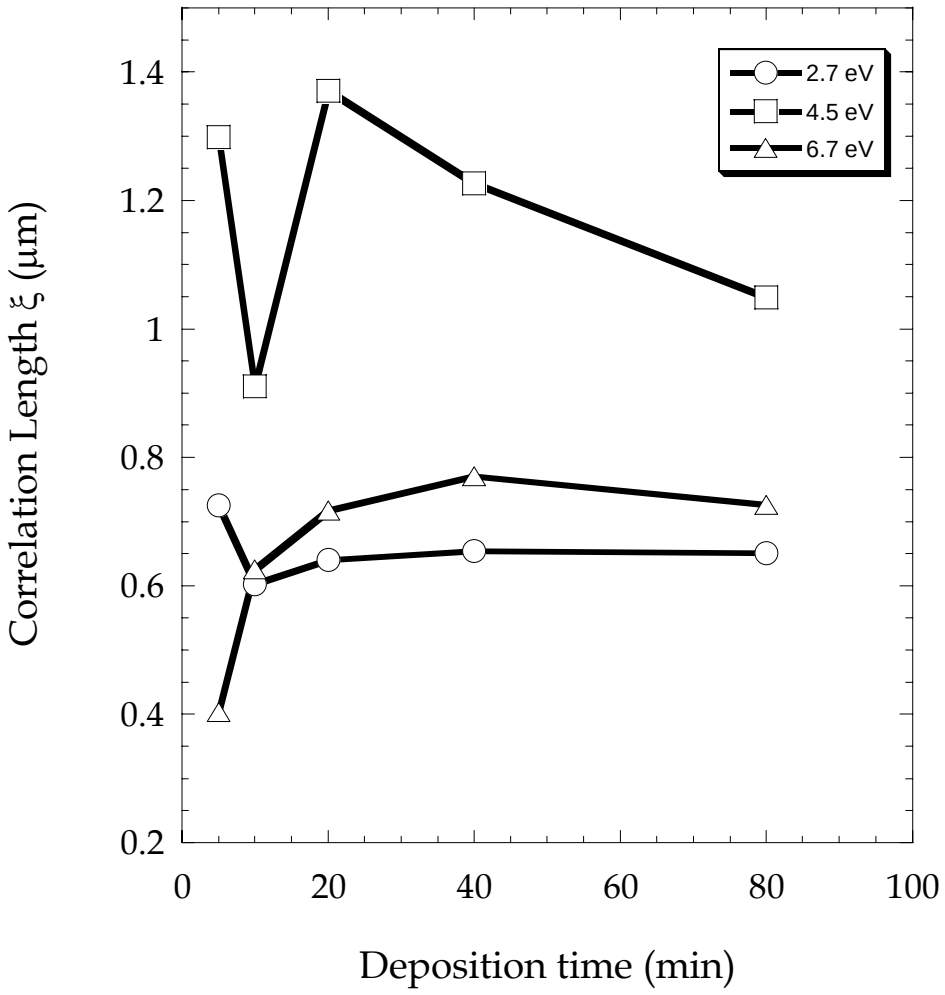

Figure 4-9 Correlation length obtained from one-dimensional power spectral density (1DPSD) analysis of AFM images plotted as a function of deposition time for pentacene thin films deposited on SiO_2 for four incident kinetic energies at normal incidence.

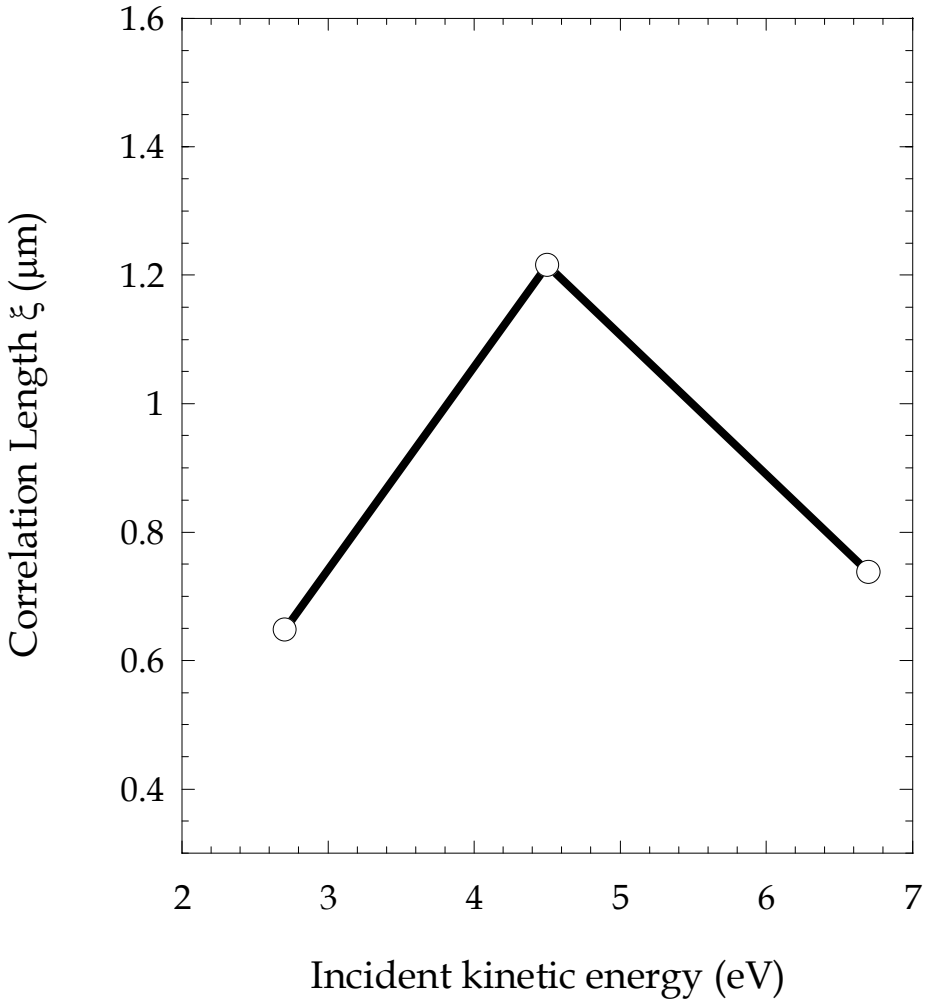

Figure 4-10 Thickness averaged correlation length from 1DPSD analysis of AFM images plotted as a function of incident kinetic energy for pentacene thin films deposited on SiO_2 modified with OTS.

5 Appendices

5.1 Contact angle

All run performed during this series of experiments were deposited on only two different Si (100) wafers. Contact angle measurements were taken for each substrate used in order to determine the reproducibility of the SAM and to compare their hydrophobicities to previously recorded results on different surfaces. These measurements employed a NRL CA goniometer (Rame-Hart Inc., Mountain Lakes, NY) with an advancing droplet volume of at least 3 μL and a receding droplet volume of about 2 μm. Each sample was analyzed at four different points to ensure sample uniformity and each droplet was measured on both sides.

Table 5-1 Contact angle results were carried out recording both the advancing and receding contact angle.

		Left Side of Substrate		Right Side of Substrate	
Substrate	Spot #	Advancing Angle	Receding Angle	Advancing Angle	Receding Angle
1.5 eV, 2.7 eV	1.	101	91	97	91
	2.	102	92	104	92
	3.	101	94	104	94
	4.	100	93	104	94
4.5 eV, 6.7 eV	1.	97	90	99	91
	2.	98	91	98	89
	3.	98	94	101	90
	4.	98	91	100	91

5.2 Constant growth rate calibration

Calibrations were carried out on the G-line system in order to attain a constant growth rate for each of the four energies; 1.5 eV, 2.7 eV, 4.5 eV, and 6.7 eV. The variable in these runs was the bubbler temperature. The calibration consisted of a run at each energy with each run containing three depositions, one deposition at each of the three bubbler temperatures.

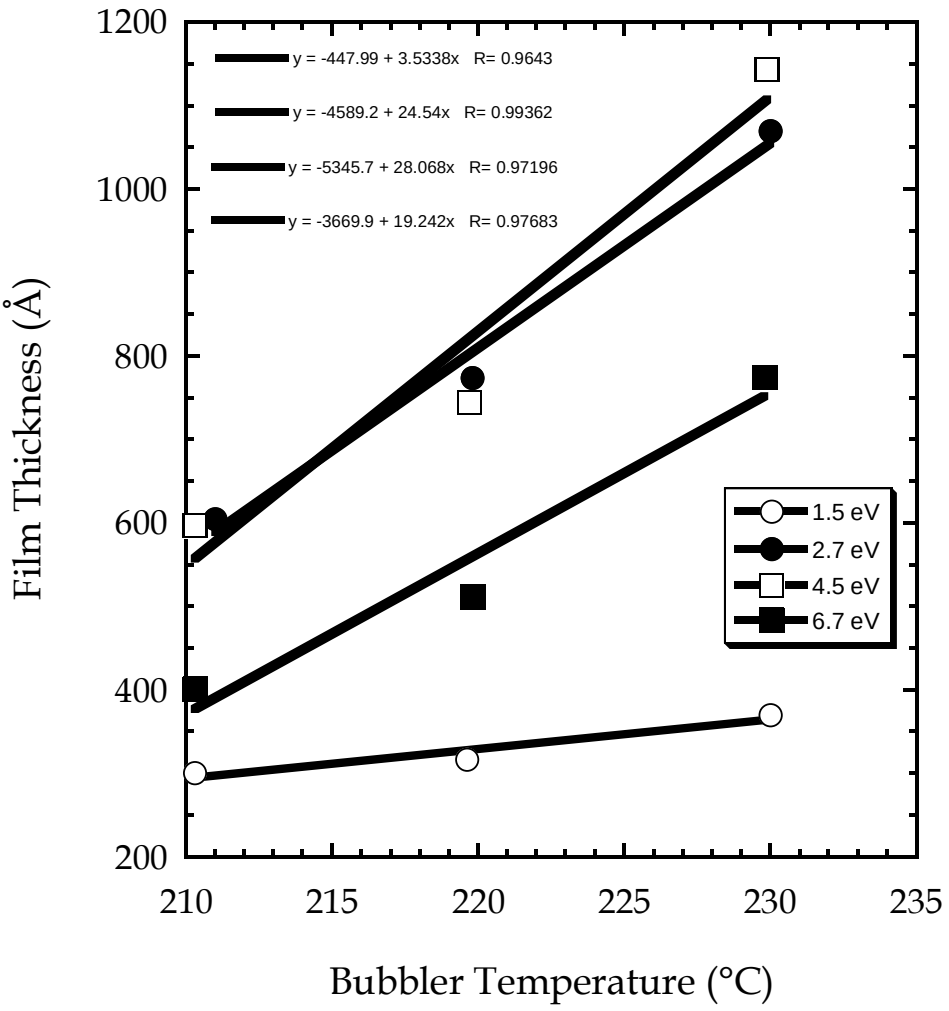

Figure 5-1 Constant growth rate calibrations were made prior to first terrace experiments on G-Line system.

6 References

[1] G. E. Moore, *Electronics* **38** (1965)

[2] C. D. Dimitrakopoulos, A. R. Brown, and A. Pomp, *J. Appl. Phys.*, **80**, 2501 (1996)

[3] Ali Afzali, Christos D. Dimitrakopoulos, and Tricia L. Breen, *J. Am. Chem. Soc.* **124,** 8812 (2002)

[4] C. W. Tang, S. A. Van Slyke, *Appl. Phys. Lett.*, **51**, 913 (1987)

[5] J. H. Burroughes, D. D. Bradley, A. R. Brown, R. N. Marks, K. Mackay, R. H. Friend, P. L. Burn, A. B. Holmes, *Nature,* **347**, 539 (1990)

[6] F. Ebisawa, T. Kurokawa, S. Nara, *J. Appl. Phys*, **54**, 3255 (1983)

[7] K. Kudo, M. Yamashina, T. Moriizumi, *Jpn. J. Appl. Phys*, **23**, 130 (1984)

[8] Y. Lin, D. Gundlach, S. Nelson, T. Jackson, *IEEE Electron Device Lett.*, **18**, 606 (1997)

[9] Silinsh, E. A., *Organic Molecular Crystal. Their Electronic States*, Springer-Verlag: Berlin, (1980)

[10] R. B. Campbell, J. M. Robertson, and J. Trotter, *Acta Crystallogr.*, **15**, 289 (1962)

[11] D. Holmes, S. Kumaraswamy, A. J. Matzger, and K. P. C. Vollhardt, *Chem.-Eur. J.*, **5**, 3399 (1999)

[12] C. D. Dimitrakopoulos, A. R. Brown, and A. Pomp, *J. Appl. Phys.*, **80**, 2501 (1996)

[13] J. B. Brzoska, I. Ben Azouz, and F. Rondelez, *Langmuir*, **10**, 4367 (1994)

[14] D. J. Gundlach, C. C. Kuo, C. D. Sheraw, J. A. Nichols, and T. N. Jackson, *Proceedings of the SPIE*, **4466**, 54

[15] R. Ruiz, B. Nickel, N. Koch, L. C. Feldman, R. F. Haglund, *Phys. Rev. B*, **67**, 125406 (2003)

[16] A. S. Killampalli, Ph.D thesis, Cornell University, 2006

[17] T. W. Schroeder, Ph.D thesis, Cornell University, 2004

[18] A. –L. Barabasi and H. E. Stanley, *Fractal Concepts in Surface Growth*, (Cambridge University Press, Cambridge, United Kingdom, 1995)

[19] Z. –W. Lai and S. Das Sarma, *Phys. Rev. Lett*. **66**, 2348 (1991)